

Carbon-Enhanced Metal-Poor Stars. III. Main-Sequence Turn-Off Stars from the SDSS/SEGUE Sample¹

Wako Aoki^{2,3}, Timothy C. Beers⁴, Thirupathi Sivarani⁴, Brian Marsteller^{4,5}, Young Sun Lee⁴, Satoshi Honda^{2,6}, John E. Norris⁷, Sean G. Ryan⁸, Daniela Carollo^{9,10}

ABSTRACT

The chemical compositions of seven Carbon-Enhanced Metal-Poor (CEMP) turn-off stars are determined from high-resolution spectroscopy. Five of them are selected from the SDSS/SEGUE sample of metal-poor stars. Another star, also chosen from the SDSS/SEGUE sample, has only a weak upper limit on its carbon abundance obtained from the high-resolution spectrum. The effective temperatures of these objects are all higher than 6000 K, while their metallicities, parametrized by $[\text{Fe}/\text{H}]$, are all below -2 ; the star with the lowest iron abundance in this study has $[\text{Fe}/\text{H}] = -3.1$. Six of our program objects exhibit high abundance ratios of barium ($[\text{Ba}/\text{H}] > +1$), suggesting large contributions of the products of former AGB companions via mass transfer across binary systems. One star in our study (SDSS 1707+58) exhibits a rapid variation in its radial velocity, which is a strong signature that this star belongs to a close binary. Combining our results with previous studies provides a total of 20 CEMP main-sequence

¹Based on data collected at the Subaru Telescope, which is operated by the National Astronomical Observatory of Japan.

²National Astronomical Observatory, Mitaka, Tokyo, 181-8588 Japan; email: aoki.wako@nao.ac.jp

³Department of Astronomical Science, The Graduate University of Advanced Studies, Mitaka, Tokyo, 181-8588 Japan

⁴Department of Physics and Astronomy, CSCE: Center for the Study of Cosmic Evolution, and JINA: Joint Institute for Nuclear Astrophysics, Michigan State University, East Lansing, MI 48824-1116; email: beers@pa.msu.edu, marsteller@pa.msu.edu, thirupathi@pa.msu.edu

⁵present address: Department of Physics & Astronomy, University of California, Irvine, Irvine, CA 92697-4575; email: marsteller@pa.msu.edu

⁶present address: Gunma Astronomical Observatory, Takayama, Agatsuma, Gunma 377-0702, Japan; honda@astron.pref.gunma.jp

⁷Research School of Astronomy and Astrophysics, The Australian National University, Mount Stromlo Observatory, Cotter Road, Weston, ACT 2611, Australia; email: jen@mso.anu.edu.au

⁸Centre for Astrophysics Research, STRI and School of Physics, Astronomy and Mathematics, University of Hertfordshire, College Lane, Hatfield AL10 9AB, United Kingdom; email: s.g.ryan@herts.ac.uk

⁹INAF – Osservatorio Astronomico di Torino, 10025 Pino Torinese, Italy

¹⁰present address: Research School of Astronomy and Astrophysics, The Australian National University, Mount Stromlo Observatory, Cotter Road, Weston, ACT 2611, Australia; email: carollo@mso.anu.edu.au

turn-off stars for which the abundances of carbon and at least some neutron-capture elements are determined. Inspection of the $[C/H]$ ratios for this sample of CEMP turn-off stars show that they are generally higher than those of CEMP giants; their dispersion in this ratio is also smaller. We take these results to indicate that the carbon-enhanced material provided from the companion AGB star is preserved at the surface of turn-off stars with no significant dilution, which appears counter to expectations if processes such as thermohaline mixing have operated in unevolved CEMP stars. In contrast to the behavior of $[C/H]$, a large dispersion in the observed $[Ba/H]$ is found for the sample of CEMP turn-off stars, suggesting that the efficiency of the s-process in very metal-poor AGB stars may differ greatly from star to star. Four of the six stars from the SDSS/SEGUE sample exhibit kinematics that are associated with membership in the outer-halo population, a remarkably high fraction.

Subject headings: nuclear reactions, nucleosynthesis, abundances – stars: abundances – stars: AGB and post-AGB – stars: Population II

1. Introduction

Abundance studies of very metal-poor (VMP; $[Fe/H] < -2.0$)¹ stars have been pursued over the past few decades in order to constrain models of nucleosynthesis, stellar evolution, and early chemical enrichment in the Galaxy (e.g., Beers & Christlieb 2005). One important result of these studies is the discovery of Carbon Enhanced Metal-Poor (CEMP) stars, which appear with increasing frequency at lower metallicity (Beers et al. 1992; Beers & Christlieb 2005; Lucatello et al. 2006; Marsteller 2007). These stars may be closely related to carbon stars in the Galactic halo, known as CH stars (Keenan 1942) and subgiant CH stars (Bond 1974).

Recent chemical abundance studies for CEMP stars have revealed that most (70–80%) CEMP stars also exhibit excesses of s-process elements such as Ba (the CEMP-s stars, according to Beers & Christlieb 2005), indicating that the origin of the carbon excesses in these stars is likely to be the triple- α reaction in Asymptotic Giant Branch (AGB) stars (e.g., Aoki et al. 2007). The CEMP stars that are observed at present are likely to have been polluted by the transfer of carbon-enhanced material from a (former) AGB companion across a binary system, while the AGB star itself has now evolved to an unseen white dwarf (e.g., Lucatello et al. 2005). Thus, the abundance patterns of heavy elements in these stars provide useful constraints on models for s-process nucleosynthesis in AGB stars. On the order of 20% of CEMP stars exhibit no significant enhancement of their neutron-capture elements (the CEMP-no stars, according to Beers & Christlieb 2005), suggesting the existence of other possible origins for their carbon excesses (e.g., Norris et al. 1997b; Aoki et al. 2002a). Aoki et al. (2007) have shown that the CEMP-no stars generally occur at very low $[Fe/H]$;

¹ $[A/B] = \log(N_A/N_B) - \log(N_A/N_B)_\odot$, and $\log \epsilon_A = \log(N_A/N_H) + 12$ for elements A and B.

extreme examples of this class of stars include HE 0107–5240 and HE 1327–2326, two hyper metal-poor (HMP) stars with $[\text{Fe}/\text{H}]$ below -5.0 (Christlieb et al. 2002; Frebel et al. 2005) and having very large carbon excesses ($[\text{C}/\text{Fe}] \sim +4$), as well as the recently identified ultra metal-poor (UMP; $[\text{Fe}/\text{H}] = -4.8$) star HE 0557-4840, with $[\text{C}/\text{Fe}] = +1.6$ (Norris et al. 2007).

Among the CEMP stars for which chemical compositions have been obtained from high-resolution spectroscopy, main-sequence turn-off stars are expected to be of particular importance. In the case of mass transfer in binary systems, the accreted material from the primary AGB star has been mixed at least by the first dredge-up in red giants, while turn-off stars might preserve pure material accreted from the primary at their surfaces. In such cases, one can investigate the efficiency of the production of carbon and neutron-capture elements in AGB stars from abundance measurements of the secondary star. Another interesting view arises from the suggested influence of so-called thermohaline mixing (Charbonnel & Zahn 2007; Stancliffe et al. 2007; Denissenkov & Pinsonneault 2007), which provides the possibility of mixing the accreted surface material while the observed star is still on the main-sequence or only slightly evolved, prior to first dredge-up. In this scenario, the contrast of the observed surface abundances of CEMP turn-off stars with more evolved CEMP stars also provides valuable clues to the nature of this proposed extensive mixing process.

Very large new samples of CEMP stars have recently become available, discovered during the course of the Sloan Digital Sky Survey (SDSS; York et al. 2000; Adelman-McCarthy et al. 2007). Although originally designed as an extragalactic survey, SDSS has also discovered large numbers of VMP stars (Beers et al. 2006). Although some of the CEMP stars are the result of directed studies (Margon et al. 2002; Downes et al. 2004), many of them have appeared among the calibration objects used by SDSS to obtain spectrophotometric and telluric corrections for other spectroscopic data. These calibration stars are primarily brighter, metal-poor main-sequence turn-off F- and G-type stars. The ongoing extension to SDSS, SDSS-II (which includes the program SEGUE: Sloan Extension for Galactic Understanding and Exploration), is expected to provide tens of thousands of additional VMP stars, at least several thousand of which are expected to be CEMP stars. This paper reports the first application of abundance measurements obtained with high-resolution spectroscopy for CEMP star candidates found by the SDSS/SEGUE surveys.

In §2 we discuss the identification of our sample stars and the observations that were carried out. A description of our analysis techniques and results is provided in §3. In §4 we present a discussion of our findings. The interesting kinematics of the SDSS/SEGUE CEMP turn-off stars are discussed in §5. We conclude with a few remarks in §6.

2. Sample Selection and Observations

The Sloan Digital Sky Survey uses a CCD camera (Gunn et al. 1998) on a dedicated 2.5m telescope (Gunn et al. 2006) at Apache Point Observatory, New Mexico, to obtain images in

five broad optical bands (*ugriz*; Fukugita et al. 1996) over approximately 10,000 deg² of the high Galactic latitude sky. The survey data-processing software measures the properties of each detected object in the imaging data in all five bands, and determines and applies both astrometric and photometric calibrations (Pier et al. 2003; Lupton et al. 2001; Ivezić et al. 2004). Photometric calibration is provided by simultaneous observations with a 20-inch telescope at the same site (Hogg et al. 2001; Smith et al. 2002; Stoughton et al. 2002; Tucker et al. 2006).

2.1. Sample selection and photometry data

During the development of pipeline software for the determination of atmospheric parameters (T_{eff} , $\log g$, $[\text{Fe}/\text{H}]$) for stars with available photometry and spectroscopy from SDSS and SEGUE (the SEGUE Stellar Parameter Pipeline; SSPP, see Lee et al. 2007a,b), it was noticed that a rather large number of stars were present in the SDSS/SEGUE database with clearly enhanced CH G-band strengths, and which were likely to be CEMP stars. A list of over 1000 candidate CEMP stars was assembled, drawing in particular on the calibration stars used by SDSS. The sample formed the basis for a detailed investigation of the frequency of CEMP stars in the SDSS database (see Marsteller et al. 2006; Marsteller 2007).

A handful of the brighter examples of the CEMP turn-off stars were identified for carrying out a pilot study of their high-resolution spectroscopic abundances, reported on herein. The imaging procedures used during the course of SDSS are tuned for extragalactic observations. As a result, there exists a bright limit corresponding to $g \sim 14.5$. Thus, the stars available for our study are somewhat faint for high-resolution abundance analyses, even with 8 m-class telescopes.

The targets for the present observing program are listed in Table 1. Figures 1 and 2 show the medium-resolution ($R = \lambda/\delta\lambda \sim 2000$) SDSS spectra of the targets. In addition to our primary objects, we selected two well-known CEMP turn-off stars, LP 706–7 (Norris et al. 1997a) and CS 29526–110 (Aoki et al. 2002c), as comparison stars.

The effective temperatures are primarily estimated from adopted $(V - K)_0$ colors (see § 3). The photometric data and reddening corrections used in this work are listed in Table 2. For the SDSS/SEGUE stars the optical photometry information (B and V) are obtained from the SDSS photometric system, employing the following empirical transformations, obtained by comparison with existing photometry for HK survey stars and subsequently observed by SDSS (Zhao & Newberg 2006):

$$V = g - 0.561(g - r) - 0.004$$

$$B = g + 0.348(g - r) + 0.175$$

The photometric data for the comparison stars are taken from Beers et al. (2007). The K pho-

tometry is obtained from the 2MASS catalogue (Skrutskie et al. 2006). The interstellar reddening is estimated from the dust map of Schlegel et al. (1998); the extinction in the V and K bands is obtained from the reddening relation provided in their Table 6.

2.2. High-resolution spectroscopy

High-resolution spectroscopy was obtained with the Subaru Telescope High Dispersion Spectrograph (HDS; Noguchi et al. 2002) in September 2006 and February 2007. Our spectra cover the wavelength range from 4050 to 6800 Å, with a gap between 5350 and 5450 Å due to the separation between the two detectors. A two-by-two pixel on-chip binning procedure was applied. The resolving power of the spectra obtained in 2006 is $R = 60,000$ (using a slit width of $0.6''$), while that obtained during the 2007 run is somewhat lower ($R = 45,000$) because a wider slit width ($0.9''$) was applied in order to collect sufficient photons under relatively poor seeing conditions. The total exposure times are listed in the third column of Table 1. It was immediately obvious, during the course of the observing run, that SDSS 1707+58 exhibited a rapid variation in its radial velocity. The exposure times for individual exposures for this object are listed separately in Table 3. The total exposure time for this object in Table 1 is the value for the spectrum used in the abundance analysis (see § 3).

Data reduction was carried out using standard procedures within IRAF². Cosmic-ray hits were removed using the procedure described by Aoki et al. (2005). The wavelength scale was determined using Th-Ar arc spectra obtained during the observing nights. Examples of the spectra around 5170 Å are shown in Figure 3. The photon counts per pixel (0.031 Å) collected at 5100 Å in the final spectra are listed in Table 1.

2.3. Equivalent widths

The equivalent widths of atomic lines are measured by fitting Gaussian profiles to (apparently) isolated absorption features. The list of atomic lines was made using those of our recent studies for CEMP stars (Aoki et al. 2007); the values are given in Table 4.

Equivalent widths of the interstellar Na I D1 line ($\lambda 5890$) are measured from a direct integration of the absorption features. The values are given in the last line of Table 4. We estimated $E(B - V)$ from the Na I absorption by applying the correlation found by Munari & Zwitter (1997). The values are given in Table 2. The agreement between the two estimates of $E(B - V)$ is good in general. An exception is SDSS 0126+06, for which a significantly larger $E(B - V)$ is obtained from the Na I line than from the dust map of Schlegel et al. (1998). This is discussed in §3.6.

²IRAF is distributed by the National Optical Astronomy Observatories, which is operated by the Association of Universities for Research in Astronomy, Inc. under cooperative agreement with the National Science Foundation.

2.4. Radial velocities

Radial velocities for our program stars are measured from the wavelengths of clean Fe lines; results are given in Table 1. The random errors of the measurements are estimated from $\sigma_v N^{-1/2}$, where σ_v is the standard deviation of the values from individual lines and N is the number of lines used for the measurement. Note that the reported error for the SDSS 0817+26 value is substantially larger than for the rest of our targets, because of the low S/N ratio of the spectrum and the small number of Fe lines used (5 lines).

Figure 4 shows the radial velocities of LP 706–7 and CS 29526–110 obtained by the present work, along with additional measurements obtained during recent service observing runs with the Subaru Telescope. For LP 706–7, the results of Norris et al. (1997a) are also shown. A clear variation of radial velocity is found for CS 29526–110, indicating that this object belongs to a binary system, although the orbital period is still unclear. On the other hand, no evidence of variability is obtained for LP 706–7, as has been discussed by Norris et al. (1997a), even though we have now obtained data extending over a range of some 6000 days.

It was immediately noticed during the first observing night of 2007 that significant variations existed in the observed Doppler shift of SDSS 1707+58. Figure 5 shows the spectra of this object before any shifts have been obtained prior to co-addition for later analysis. No velocity variation is found for the Na I D emission lines associated with the Earth’s atmosphere at 5989.9 and 5995.9 Å, nor for the interstellar absorption feature due to Na, found about 0.5 Å blueward of these emission lines, indicating that the wavelength calibration was correctly carried out over all exposures. In contrast, absorption due to the stellar Na I features quickly shifted in the spectra obtained in the first observing night (the upper three spectra in the Figure), while no significant variation is found for those obtained during the second night. We note that the exposure times applied to the first and second observing nights are 40 and 20 minutes, respectively. The shift in the first night is about 18 km s⁻¹ per 40 minutes. Hence, the broad absorption features of the first three spectra are almost certainly due to a radial velocity shift during the exposures rather than stellar rotation or macro-turbulence.

The radial velocities and line widths measured for each spectrum of SDSS 1707+58 are listed in Table 3. The measurements are made for strong Na I, Mg I, and Ba I lines, because measurements from the Fe I lines for individual exposures were quite uncertain. During the course of this procedure, it was decided to exclude the third spectrum obtained during the second night because of significant contamination from the twilight sky. The UT and JD (heliocentric Julian day) of the central time of each exposure is listed in the Table. A spectrum of this object, suitable for carrying out the abundance analysis described below, is obtained by combining individual spectra obtained during the first night, after applying the appropriate Doppler corrections.

Radial velocities are also measured from the SDSS spectra, as listed in Table 5. The radial velocities of SDSS 0036–10, SDSS 0126+06, and SDSS 0924+40 agree with the results from the Subaru spectra within the measurement errors. The radial velocity of SDSS 2047+00 on JD =

2,452,932 is significantly higher than the other three measurements, suggesting a radial velocity variation and binarity of this object. We note that this object shows large over-abundances of carbon and neutron-capture elements (§3) that are expected from mass transfer in a binary system. The radial velocity of SDSS 1707+58 from the SDSS spectrum is within the variation found in the Subaru spectra given in Table 3. Finally, the radial velocity of SDSS 0817+26 from the SDSS spectrum, $45.8 \pm 3.5 \text{ km sec}^{-1}$, is much higher than the value obtained from the HDS spectrum. However, the measurement is only once for each instrument, so further measurement is required to derive any firm conclusions on the binarity of this object.

3. Chemical Abundance Analysis and Results

3.1. Stellar parameters

We determine the effective temperatures from the $(V-K)_0$ colors using the scale of Alonso, Arribas, & Martínez (1996); these are listed in Table 2 as $T_{\text{eff}}(V-K)$. The $(V-K)_0$ values of CS 29526–110, SDSS 0036–10, SDSS 2047+00, SDSS 0126+06 and SDSS 1707+58 are slightly lower than the range for which the Alonso et al. scale (formula) is applicable ($V-K < 1.1$ for $[\text{Fe}/\text{H}] < -1.5$). For these objects, we directly estimate the effective temperature from Figure 8 of Alonso, Arribas, & Martínez-Roger (1996), in which the correlation between $V-K$ and effective temperatures for their calibration stars is shown.

The effective temperatures obtained from the $(B-V)_0$ colors using the Alonso et al. scale are also listed in Table 2. For CEMP stars, this color is sometimes severely affected by the presence of molecular absorption, and it is not preferable for temperature estimates. However, the molecular features of warm CEMP stars studied here are not as significant as those for cooler stars, and would be expected to have less of an affect on the observed colors. Moreover, the errors in the K -band photometry for some of the fainter objects in our sample are large (see below), and the $V-K$ colors are relatively sensitive to the reddening correction. Hence, the effective temperatures obtained from the $(B-V)_0$ colors are useful for comparison purposes. The $T_{\text{eff}}(B-V)$ of SDSS 0036–10 and SDSS 1707+58 agree well with their $T_{\text{eff}}(V-K)$ determinations. The $T_{\text{eff}}(B-V)$ of the two coolest stars in our sample, LP 706–7 and SDSS 0924+40, are lower than their $T_{\text{eff}}(V-K)$, perhaps as the result of their relatively strong CH molecular bands affecting the B -band measurement. A similar discrepancy between the two T_{eff} estimates is found for SDSS 0817+26, even though this object exhibits no or perhaps only a modest ($[\text{C}/\text{Fe}] \sim +1$) carbon overabundance. However, the error in the K photometry for this star is relatively large, which might explain the discrepancy.

The $T_{\text{eff}}(V-K)$ of SDSS 2047+00 is quite high (6800 K) for a VMP turn-off star. However, the error of the K photometry (0.12 magnitudes) and the reddening correction for this star ($E(B-V) = 0.088$) are the largest among our sample. Moreover, the $T_{\text{eff}}(B-V)$ is about 200 K lower than the $T_{\text{eff}}(V-K)$. For this object we adopt $T_{\text{eff}} = 6600 \text{ K}$, which is slightly lower than the estimate from the $V-K$ color.

The T_{eff} of CS 29526–110 is also quite high (6800 K). However, the reported error of the K photometry for this object is 0.03 magnitudes, and the reddening correction adopted (0.033 magnitudes) is not large. For this object, the R and I photometry data are also available (Beers et al. 2007). The T_{eff} from $V - R$ and $V - I$ estimated using the figures of Alonso, Arribas, & Martínez-Roger (1996) are 6700–6800 K, while the $T_{\text{eff}}(B - V)$ is 6500 K. We adopt the T_{eff} from $(V - K)_0$ with no modification for this object.

We now estimate the uncertainty in the adopted T_{eff} for our program stars, taking the error in the $(V - K)_0$ colors and the error in the scale of Alonso, Arribas, & Martínez-Roger (1996) into consideration. The error of the K photometry is the dominant source of the uncertainty in the $(V - K)_0$ values for most objects. The sensitivity of T_{eff} to the color is approximately 150 K per 0.1 magnitude in $V - K$. We adopt 100 K as the errors arising from the temperature scale for stars with $(V - K)_0 \geq 1.1$, for which Alonso et al.’s formula is applicable, and 150 K for other objects, respectively. The uncertainties are 100-150 K for relatively cool or bright objects (SDSS 0817+26, SDSS 0924+40, LP 706–7, and CS 29526–110), and 150-200 K for others. The adopted errors of T_{eff} in this study are listed in Table 6.

The surface gravity, metallicity, and micro-turbulence for our program stars are determined from an analysis of the Fe I and Fe II lines, using the model atmospheres of Kurucz (1993). The micro-turbulence (v_{turb}) and gravity ($\log g$) are determined so that the derived Fe abundance is not dependent on the strengths of Fe I lines, nor on the ionization stages, respectively. An exception is SDSS 0817+26, for which the number of useful Fe I lines is too small to estimate the micro-turbulence, and no Fe II line is available to estimate the gravity. We adopted typical values ($\log g = 4.0$ and $v_{\text{micro}} = 1.5 \text{ km s}^{-1}$) found for turn-off stars³. We note that this object is excluded in the discussion of CEMP stars because its carbon abundance is not determined by our analysis of the HDS spectrum (see below); we only obtain a weak upper limit for [C/Fe]. The number of Fe I lines used in the analysis of SDSS 1707+58 is also quite small, due to the rapid changes of the radial velocity (see below). For this object, $v_{\text{micro}}=1.5 \text{ km s}^{-1}$ is also adopted. For SDSS 0126+06, a correlation between the Fe I line strengths and the derived Fe abundances is found even if $v_{\text{micro}} > 2.0 \text{ km s}^{-1}$ is assumed. Since such a high value of v_{micro} is not known in turn-off stars, we adopt $v_{\text{micro}}=2.0 \text{ km s}^{-1}$ for this object. Larger errors in the gravity ($\sigma[\log g]$) and the micro-turbulence ($\sigma[v_{\text{micro}}]$) are adopted for these objects. The atmospheric parameters adopted in the following abundance analyses and their corresponding errors are listed in Table 6.

Figure 6 shows the estimated effective temperatures and surface gravities for our sample (filled circles) along with other CEMP stars studied in previous work (open circles; see below). The lines are the isochrones by Kim et al. (2002) for [Fe/H]= -2.5 and assumed ages of 10, 12, and 14 Gyrs. Inspection of this Figure shows that our objects fall around the turn-off region for old metal-poor stars, although it is difficult to distinguish whether they are main-sequence stars or subgiants. We

³If a lower gravity ($\log g = 2.0$) is adopted for the case of a horizontal branch star, the derived iron abundance is only slightly higher, while the derived Sr and Ba abundances (see §3.3) are about 0.6 dex lower.

note that if we adopt a higher effective temperature (6800 K from $V - K$) for SDSS 2047+00, the surface gravity also becomes quite high ($\log g=4.9$), far above the expected value based on isochrones of VMP turn-off stars.

3.2. Carbon abundance

The carbon abundance estimates for our program stars are determined from spectrum synthesis of the CH 4323 Å band, as previously described by Aoki et al. (2007). The sources of molecular data are reported by Aoki et al. (2002c). The oxygen abundance of $[O/Fe]=+0.5$ is assumed in the analysis. We confirmed that the effect of assumed oxygen abundance on the derived carbon abundances is negligible for the range $0 < [O/Fe] < +2$ for a star with $T_{\text{eff}} > 6000$ K, in which the fraction of carbon bound in the CO molecule is very small.

No signature of the CH band is detected in the HDS spectrum of SDSS 0817+26, so only an upper limit is determined (note that in the medium-resolution SDSS spectrum, there is sufficient strength in this band, and others, to obtain a detection, $[C/Fe]=+1.2$; see §3.6). The determination of carbon abundance for SDSS 1707+58, based on the high-resolution spectrum alone, is very uncertain because of the relatively low S/N ratio of the spectrum. The full set of results is listed in Table 7.

Carbon abundances are also measured from the C₂ Swan band at 5165 Å for LP 706–7, SDSS 0036–10, and SDSS 0924+40. The result for SDSS 0924+40 agrees well with that obtained from the CH band, while the carbon abundances of LP 706–7 and SDSS 0036–10 from the C₂ band are slightly (0.1–0.2 dex) higher than those from the CH band, as was also found for the CEMP subgiant LP 625–44 by Aoki et al. (2002b). Although there may exist a small systematic error in the determination of carbon abundances from the C₂ band and/or from the CH band, the measurements from the C₂ band confirm the reliability of carbon abundance determination from the other molecular band.

3.3. Abundances of other elements

The abundances for most of the other elements are determined by a standard analysis based on measured equivalent widths. The effects of hyperfine splitting and isotope shifts are included in the analysis, using McWilliam (1998) for Ba, Lawler et al. (2001) for La, and Simons et al. (1989) for Pb. Solar isotope ratios are assumed for Pb. For Ba, we first measured the abundances neglecting the effect of hyperfine splitting, and then applied the isotope ratios of the r-process component in Solar System material for the two stars having $[Ba/Fe] < 1$ (SDSS 0036–10 and SDSS 0817+26), and s-process ratios for the stars that exhibit Ba excesses, as was done previously by Aoki et al. (2007).

While Sr and Ba abundances are measured for all objects in our sample, other neutron-capture elements are detected in only a few stars. The abundances of Pb, which is a key element for investigation of neutron-capture nucleosynthesis, are measured for LP 706–7, CS 29526–110, SDSS 0126+06 and SDSS 0924+40, while an upper limit is estimated for other stars. The upper limit on the Pb abundance is calculated based on the 3σ error of the equivalent-width measurement, estimated by $\sigma_W = (\lambda n_{\text{pix}}^{-1/2}) / (R[S/N])$, where R is the resolving power and n_{pix} is the number of pixels for which equivalent width measurements are carried out (Norris et al. 2001). The results are listed in Table 7.

Six of our program stars exhibit large Ba over-abundances. In particular, the over-abundance found for SDSS 1707+58 is quite striking ($[\text{Ba}/\text{Fe}] = +3.4$). This star also exhibits a large excess of Sr ($[\text{Sr}/\text{Fe}] = +2.25$). Although the carbon abundance estimated from the CH band for this object is very uncertain, we include this object in our discussion of CEMP stars as an example of a star that is likely affected by AGB nucleosynthesis (see §4).

3.4. Uncertainties

Random errors in our analysis, which include the uncertainty of the equivalent-width measurements and in the adopted transition probabilities, are estimated to be $\sigma N^{-1/2}$, where σ is the standard deviation of derived abundances from individual lines and N is the number of lines used in the analysis. When the number of lines are smaller than four, the σ of Fe I (σ_{Fe}) is adopted in the estimates. Typical random errors are 0.05–0.15 dex, depending on the number of lines used in the analysis.

We also estimate the error due to the uncertainty in equivalent-width measurements for the Fe I lines of SDSS 0036–10. A typical error in equivalent width (σ_W) is estimated from the above formula. The typical value for the Fe I lines of SDSS 0036–10 is obtained to be 3 mÅ, assuming $\lambda = 5000 \text{ \AA}$ and $S/N = 70$. We added this value to the measured equivalent widths and calculated the Fe abundance using the same model atmosphere as used in the analysis. The derived iron abundance is 0.10 dex higher than the original result. This value is comparable with the σ_{Fe} of 0.12 dex obtained for SDSS 0036–10. This result confirms that the random errors of the abundance measurements are primarily due to the uncertainties in the equivalent width measurements reflecting the quality of the spectrum, although the σ_{Fe} also includes the errors in the continuum placement and uncertainties of gf values.

The errors due to the uncertainty of the atmospheric parameters are estimated for LP 706–7 and CS 29526–110. Table 8 lists the sensitivity of the derived abundances ($\log \epsilon$ values) to the changes of parameters. For other objects in our program, the uncertainties are estimated by applying the data for the star of this pair with the closest atmospheric parameters to the object under consideration. Total uncertainties are obtained by adding these values, in quadrature, to the random errors, and are listed in Table 7.

The chemical abundances of LP 706–7 are also determined using the updated (NEWODF) ATLAS grid (Castelli & Kurucz 2003), and the differences from those based on the Kurucz (1993) model are given in Table 8 (Δ_{ATLAS}). The abundances using the NEWODF model are lower by 0.05–0.14 dex. The effect of the difference of model atmospheres on the derived abundances is systematic, and that on the abundance ratios is not significant. We also applied the model including the excesses of α elements, and confirmed the effect on the derived abundances is smaller than 0.01 dex.

Further systematic errors could exist in our LTE analysis based on one-dimensional (1D) model atmospheres. The non-LTE correction for Fe abundances derived from the Fe I lines might be the order of +0.2 dex (Collet et al. 2005; Asplund 2005a, and references therein), although the values estimated are different between authors. The direction of the correction for the 3D effect is opposite (Asplund 2005a). The most significant 3D effect would appear in the carbon abundances determined from CH molecular features, that could reach to -0.7 dex in the most metal-poor cases (Collet et al. 2006). In order to obtain the corrections for these effect, 3D analyses based on non-LTE calculation are required.

3.5. Comparison with previous studies

The elemental abundances of LP 706–7 (= CS 31062–012) and CS 29526–110 were studied by Aoki et al. (2002b) and Aoki et al. (2002c). The atmospheric parameters adopted by them for LP 706–7 are $T_{\text{eff}} = 6250$ K, $\log g = 4.5$, $[\text{Fe}/\text{H}] = -2.55$, and $v_{\text{micro}} = 1.5$ km s $^{-1}$, which are quite similar to those in the present study. Although the previous studies are based on a spectrum covering only a blue range of wavelengths, and the spectral line set used in the previous analyses is different from that in the present study, the derived abundances of most elements agree within 0.1 dex. The Cr abundance shows the largest discrepancy, on the order of 0.17 dex, which is still within the 2σ range of the measurement errors.

The effective temperature of CS 29526–110 adopted by Aoki et al. (2002c) is 300 K lower than that of the present analysis. The discrepancy of $[\text{Fe}/\text{H}]$ between the two measurements (0.32 dex) is well explained by the difference in the adopted effective temperatures. The $[\text{C}/\text{Fe}]$ values, after correction for the difference in effective temperatures, also agree within the measurement errors. The abundance ratios of other elements ($[\text{X}/\text{Fe}]$) are relatively insensitive to the effective temperature (see Table 8). It is clear that the results for Cr and Ni from the two studies exhibit significant discrepancies. However, the measurements for these elements are based on only one line for each; the results might not be expected to be as reliable as those for other elements. The $[\text{Ba}/\text{Fe}]$ derived from the present work is 0.28 dex higher than that of Aoki et al. (2002c). This result is not explained by the differences of adopted atmospheric parameters. While the previous measurement is based on only the two very strong resonance lines, our present analysis added two red lines which are suitable for abundance determination, so the new measurement should be more reliable than the previous one.

3.6. Comparison with the estimates from SDSS/SEGUE spectra

Table 9 provides a comparison of the atmospheric parameters and carbon abundances between the estimates obtained from the SDSS spectra and the present measurements.

For the SDSS spectra, we begin by adopting the stellar parameters obtained by the SSPP (Lee et al. 2007a,b). Based on these, we generate synthetic spectra for each star in the region between 4200–4400 Å. The model atmospheres used are the NEWODF models of Castelli & Kurucz (2003). The synthetic spectra are generated using the turbospectrum synthesis code (Alvarez & Plez 1998), which employs line broadening according to the prescription of Barklem & O’Mara (1998) and Barklem & Aspelund-Johansson (2005). The atomic line data are taken mainly from the VALD compilation (as of 2002) (Kupka et al. 1999), and updated from the literature, whenever possible. The molecular species CH and CN are provided by B. Plez (Plez & Cohen 2005). We adopted the solar abundances by Asplund, Grevesse & Sauval (2005a). The synthetic spectra are generated with a initial resolving power $R = 10^6$, then were smoothed to the SDSS resolution and rebinned to 1 Å pixels.

We find the best match to the region around the G band (4323 Å and 4325 Å) by changing the carbon abundance of the synthetic spectra in order to minimize the discrepancy with the observed spectra. We estimate that the errors in the derived [C/Fe] arising from errors in the stellar parameters from the SSPP is on the order of 0.35 dex.

The effective temperatures derived from the SDSS spectra agree with the values adopted by the present work, based on colors, to within about 100 K. An exception is that for SDSS 0126+06, for which the SDSS estimate is 370 K higher than the value adopted in the above analysis. For this object, larger interstellar reddening is derived from the Na I absorption than from the dust map that is adopted in the analysis (§ 2.3). If the $E(B - V)$ from the Na I measurement is adopted, the T_{eff} is as high as 7000 K, and agrees with the estimate from the SDSS spectrum.

In contrast to the agreement of effective temperatures, $\log g$ values estimated from SDSS spectra are systematically lower than those determined by our analyses from Subaru spectra. Although the results for SDSS 0126+06 from the two estimates appear to agree well, a similar discrepancy would result if the same effective temperature is adopted in the estimate of gravity. Although further study or calibration to resolve the discrepancy is desired, it should be noted that the $\log g$ values from SDSS spectra are already useful to estimate the evolutionary status of the targets (i.e., in order to distinguish giants and main-sequence turn-off stars).

The abundance ratios [Fe/H] and [C/Fe] from the two measurements agree fairly well, as found in Table 9. The discrepancy in [Fe/H] for SDSS 0126+06 (0.4 dex) is well explained by the difference in the estimated T_{eff} . No CH absorption feature is detected in the Subaru spectrum of SDSS 0817+26. A very weak CH band is found in the SDSS spectrum of this object (see Figure 2), and we have derived [C/Fe] = $+1.19 \pm 0.35$, based on its strength. Marsteller (2007) estimated that the detection limit of the CH feature in SDSS spectra can be as high as [C/H] ~ -1 for stars

with $T_{\text{eff}} \sim 6300$ K. Thus, SDSS 0817+26 could also be mis-identified as a carbon-enhanced object in our sample selection, which was carried out before detailed investigations for SDSS sample were made. Further calibrations, or strict estimates for the detection limits of CH absorption in SDSS spectra as a function of T_{eff} , are desired for more efficiently selecting carbon-enhanced objects from SDSS/SEGUE spectra.

4. Discussion

4.1. Elemental abundances of CEMP turn-off stars

The present analysis has obtained elemental abundances for five new CEMP stars selected from the SDSS/SEGUE surveys, as well as for two known CEMP stars. The remaining program star in our sample (SDSS 0817+26) is excluded from the following discussion, because no clear excess of carbon nor neutron-capture elements has been found in the high-resolution spectrum. All seven CEMP stars are classified as main-sequence turn-off stars, with $T_{\text{eff}} > 6000$ K. In order to better investigate the nature of such stars, we have compiled all known CEMP stars from the literature having T_{eff} higher than 6000 K (Table 10). In this section, we discuss the abundance distributions of carbon and the neutron-capture elements for these CEMP turn-off stars.

4.2. Distribution of C and Ba abundances

Figure 7 shows the C and Ba abundance ratios as a function of $[\text{Fe}/\text{H}]$. All objects but one exhibit very large excesses of C ($[\text{C}/\text{Fe}] \gtrsim +2$). The exception is CS 29528–041, which has $[\text{C}/\text{Fe}] = +1.59$ at $[\text{Fe}/\text{H}] = -3.25$ (Sivarani et al. 2006). Excluding this object, a clear correlation is found between $[\text{C}/\text{Fe}]$ and $[\text{Fe}/\text{H}]$. The correlation indicates that there exists a constant $[\text{C}/\text{H}]$ among these stars.

Figure 8 is a histogram of the $[\text{C}/\text{H}]$ values for the CEMP turn-off stars. The distribution is compared with that of the 31 CEMP giants selected from Aoki et al. (2007) that have $\log L/L_{\odot}$ higher than 1.5, where L is the luminosity estimated from the stellar parameters assuming a constant stellar mass (see Aoki et al. 2007). The Ba-enhanced (CEMP-s) stars are shown by open bars, while Ba-normal (CEMP-no) stars are shown by the hatched bars. A glance at this figure shows that the $[\text{C}/\text{H}]$ ratios of the CEMP-s turn-off stars distribute within a narrow range around $[\text{C}/\text{H}] \sim 0$, with the exception of the one object mentioned above (CS 29528–041). The average and standard deviations of the $[\text{C}/\text{H}]$ ratios for these two CEMP-s samples are $\langle [\text{C}/\text{H}] \rangle = -0.18$ and $\sigma([\text{C}/\text{H}]) = 0.18$ for the turn-off stars, and $\langle [\text{C}/\text{H}] \rangle = -0.54$ and $\sigma([\text{C}/\text{H}]) = 0.40$ for the giants. The two objects having the lowest $[\text{C}/\text{H}]$ among turn-off stars (CS 29528–041) and giants (CS 30322–023) are excluded in the calculation of these statistics.

The lower portion of the $[\text{C}/\text{H}]$ distribution might be affected by a temperature-related selection

bias for CEMP stars identified on the basis of the CH molecular bands, which is significantly weaker in turn-off stars than in giants. Our previous investigation for the detection limit showed that the CH band of a turn-off star with $T_{\text{eff}} \sim 6400 \text{ K}$ and $[\text{C}/\text{H}] \sim -1.6$ has depths of 2%, which is a conservative detection limit in high-resolution spectra. For the carbon-enhanced stars selected from the lower-resolution spectra, such as the SDSS/SEGUE sample, Marsteller (2007) estimated that the selection of CEMP stars from the CH band is complete for stars having $[\text{C}/\text{H}] = -1$ and $= -0.3$ for stars with $T_{\text{eff}} = 6000$ and 6500 K , respectively. Hence, in order to investigate the complete distribution of $[\text{C}/\text{H}]$ for turn-off stars, abundance studies of candidate metal-poor stars that are selected regardless of their CH band strengths in medium-resolution spectra are required. Note, however, that the sample of CEMP turn-off stars in Table 10 includes stars with T_{eff} as low as 6000 K , and that several stars were observed on programs that did not focus on carbon-enhanced stars (e.g. Cohen et al. 2004). The absence of stars with $-1 < [\text{C}/\text{H}] < -0.5$ in the sample of CEMP turn-off stars suggests that such stars are rare compared with CEMP stars with higher $[\text{C}/\text{H}]$ values. We note that we cannot derive any conclusion for the lower $[\text{C}/\text{H}]$ range ($[\text{C}/\text{H}] < -1.0$). There may well exist a number of CEMP turn-off stars that have not yet been identified by the surveys to date. This range is particularly important for studies of the Ba-normal CEMP stars, as discussed by Aoki et al. (2007).

Aoki et al. (2007) showed that the $[\text{C}/\text{H}]$ distribution for 54 CEMP stars with Ba excesses, including turn-off stars, subgiants, and giants, exhibits a peak in the range $-0.5 < [\text{C}/\text{H}] < 0.0$, and a cut-off at $[\text{C}/\text{H}] \sim 0$. This was interpreted as an indication that (1) the $[\text{C}/\text{H}]$ ratios produced by AGB stars are almost constant at $[\text{C}/\text{H}] \sim 0$, independent of metallicity, and (2) the carbon-enhanced material transferred from AGB stars to the companion is directly observed, or is only slightly diluted through the evolution from turn-off stars to giants. In this study we confirmed the absence of objects having $[\text{C}/\text{H}] \gg 0$, found that the average of the $[\text{C}/\text{H}]$ values for CEMP turn-off stars is higher than that of giants, and that their dispersion is smaller. This result supports the interpretation of Aoki et al. (2007).

Stancliffe et al. (2007) investigated the process of thermohaline mixing in main-sequence stars that received carbon-enhanced material from a companion AGB star across a binary system. They predicted that the accreted material quickly mixes throughout 90% of the star, and that the enhanced carbon is diluted in main-sequence stars as a result. The C abundance is predicted to change only slightly after the receiving star evolves through first dredge-up. This is not supported by the comparison of $[\text{C}/\text{H}]$ distributions in Figure 8, although the possible bias in the sample selection could slightly affect the comparison. Our present observational result suggests that the $[\text{C}/\text{H}]$ ratios measured for turn-off stars represents the values produced by the donor AGB stars, and the surface carbon abundance decreases in some CEMP stars during their evolution after the first dredge-up⁴. It should be noted that the $[\text{C}/\text{H}]$ values found in CEMP turn-off stars (i.e. $[\text{C}/\text{H}] \sim 0$) agree

⁴One possible interpretation is that the mass accreted from AGB stars is much larger than that assumed in the models of Stancliffe et al. (2007) in most cases, and the dilution in main-sequence stars is not as significant as

well with predictions from AGB models (e.g. van den Hoek & Groenewegen 1997), as discussed by Aoki et al. (2007). This agreement supports the above interpretation.

The carbon excesses of CS 29528–041 and CS 30322–023 are exceptionally small among the sample of CEMP turn-off stars and giant stars, respectively⁵. It is noteworthy that these two stars both exhibit very large excesses of nitrogen – the $[N/Fe]$ of CS 29528–041 is +3.0 (Sivarani et al. 2006) and that of CS 30322–023 is +2.8 (Masseron et al. 2006). Their $[(C+N)/H]$ values are -0.9 and -1.3 , respectively, which are not by far lower than those of other stars, although the nitrogen abundances are not determined for several stars including our SDSS sample. CS 30322–023 is a highly evolved giant, and possibly presently in the AGB stage (according to Masseron et al.); its surface composition could have been altered significantly during its evolution. The observed nitrogen excess of CS 29528–041 should instead be a direct result of the nucleosynthesis in a donor AGB star. As discussed by Sivarani et al. (2006), CS 29528–041 might have been polluted by an intermediate-mass AGB star in which nitrogen is enriched by the hot bottom burning process.

4.3. Neutron-capture elements

Based on their observed $[C/H]$ distribution, we have interpreted the surface abundances of CEMP turn-off stars to represent the yields of the AGB donors. If this is indeed the case, $[Ba/H]$ can be used as an indicator of the s-process efficiency in the donor stars. Figure 9 depicts the distribution of $[Ba/H]$ for the CEMP turn-off stars and giants that show excesses of Ba ($[Ba/Fe] > +0.5$). The $[Ba/H]$ of the turn-off stars exhibits a wider distribution than was observed for their $[C/H]$. The average and standard deviation of the $[Ba/H]$ for the 16 CEMP turn-off stars discussed in the context of their $[C/H]$ are $\langle[Ba/H]\rangle = -0.25$ and $\sigma([Ba/H]) = 0.68$ dex, respectively. The wider distribution of $[Ba/H]$ of these stars, as compared to $[C/H]$, implies that the Ba abundances produced by AGB stars are likely to have a significantly larger intrinsic dispersion.

The abundance ratios currently observed are those of the material transferred from the donor AGB stars, which would be dependent on the evolutionary phase in which the mass transfer occurred. The abundances of carbon and Ba are expected to increase with increasing the number of thermal pulses. Detailed comparisons with model predictions for surface abundances after each thermal pulse would be required. In such comparisons, a strong constraint is the almost constant C/H ratios found in most CEMP turn-off stars.

Figure 10 shows the $[Sr/Ba]$ and $[Ba/Pb]$ ratios of CEMP turn-off stars as a function of $[Ba/H]$.

predicted in their models.

⁵After this paper is submitted, an analysis result for the double-lined spectroscopic binary CS 22964–161 was reported by Thompson et al. (2007). The both components are CEMP turn-off stars showing large excesses of neutron-capture elements. The $[C/H]$ of this system is -1.2 , and is another example of CEMP turn-off stars having relatively low $[C/H]$ values.

Here, the three elements Sr, Ba, and Pb are regarded as representing the yields at the three abundance peaks of the s-process, corresponding to the neutron magic numbers 50, 82, and 126. The $[\text{Sr}/\text{Ba}]$ ratios are distributed over a narrow range (a standard deviation of 0.34 dex) around $[\text{Sr}/\text{Ba}] \sim -1.3$. However, they also exhibit a statistically significant anti-correlation with $[\text{Ba}/\text{H}]$ – the null hypothesis that no correlation exists between $[\text{Sr}/\text{Ba}]$ and $[\text{Ba}/\text{H}]$ is rejected by a simple t-test at the 98% confidence level. That is, the production efficiency of the heavy neutron-capture elements, with respect to the light ones, apparently increases slightly with the total production efficiency of neutron-capture elements. It should be noted that the $[\text{Sr}/\text{Ba}]$ ratios in these stars are lower than the prediction from models of the s-process in AGB stars by Busso et al. (2001): the $[\text{ls}/\text{hs}] (= -[\text{hs}/\text{ls}])$ values of their calculations, where ls and hs mean the elements in the first and second abundance peaks of the s-process, range between 0 to -1 , depending on stellar mass and choice of ^{13}C pocket, for the metallicity range of $[\text{Fe}/\text{H}] < -2$. The observations suggest more efficient production of Ba (hs), or less efficient production of Sr (ls), than model predictions.

A similar correlation was found from the abundance measurements for carbon-rich post-AGB stars by Reyniers et al. (2004). They reported a positive correlation between the enhancement of s-process elements ($[\text{s}/\text{Fe}]$, which is the mean of the abundance ratios of several s-process elements) and the abundance ratios of heavy to light neutron-capture elements ($[\text{hs}/\text{ls}]$). We note that the efficiency of the neutron-capture nucleosynthesis is represented by $[\text{s}/\text{Fe}]$ in Reyniers et al. (2004), while it is evaluated by $[\text{Ba}/\text{H}]$ in our investigation. However, a correlation between $[\text{Sr}/\text{Ba}]$ and $[\text{Ba}/\text{Fe}]$ is also found in our sample at a similar confidence level as that between $[\text{Sr}/\text{Ba}]$ and $[\text{Ba}/\text{H}]$.

The lower panel of Figure 10 suggests that there may exist a correlation for $[\text{Ba}/\text{Pb}]$ with $[\text{Ba}/\text{H}]$, but this essentially depends on only one object (HE 0024–2523), with $[\text{Ba}/\text{H}] = -1.36$ and $[\text{Ba}/\text{Pb}] = -1.84$. It should be kept in mind that the detection of Pb lines is much more difficult than those of Sr and Ba, which could result in a lack of objects having high $[\text{Ba}/\text{Pb}]$ and low $[\text{Ba}/\text{H}]$. The $[\text{Ba}/\text{Pb}]$ ratios observed are higher than the prediction from models of the s-process by Busso et al. (1999), as has been argued by previous studies (e.g. Cui & Zhang 2006). Further studies of Pb abundances, as well as modeling of the s-process to explain the discrepancy between the observations and predictions, are clearly required in order to better understand the overall neutron-capture nucleosynthesis process in AGB stars.

4.4. SDSS 1707+58: an object belonging to a close binary?

As discussed in § 2, SDSS 1707+58 exhibited a rapid variation of radial velocities on February 10, 2007, suggesting that this object belongs to a close binary system. However, it is interesting that no clear variation was found in the February 11 spectra, where the radial velocity is close to the middle of the three spectra obtained on February 10. This result could well imply a large eccentricity of the binary system, although the radial velocity measurements are still too sparse to confidently derive orbital parameters. Further radial velocity monitoring of this object is clearly desirable.

The observed excesses of neutron-capture elements in this object are very large (e.g., $[\text{Ba}/\text{Fe}] = +3.4$). Indeed, the $[\text{Ba}/\text{H}]$ value of this object is the highest among the CEMP stars shown in Figure 9. The $[\text{Sr}/\text{Ba}]$ ratio ($[\text{Sr}/\text{Ba}] = -1.15$) is a typical value found for Ba-enhanced CEMP stars (Figure 10), as compared to that of r-process-enhanced stars ($[\text{Sr}/\text{Ba}] \sim -0.4$; e.g. Sneden et al. 2003), suggesting that the neutron-capture elements of this star originated from operation of the s-process in an AGB donor star.

Lucatello et al. (2003) studied the CEMP turn-off star HE 0024–2523 ($[\text{Fe}/\text{H}] = -2.7$), which they showed to be a short-period spectroscopic binary. This star has a orbital period of 3.4 days, with a very small eccentricity (0.01). Sivarani et al. (2006) also reported a candidate CEMP turn-off close binary, CS 22958–042, for which a significant radial velocity change was found based on two exposures taken during a single observing run. SDSS 1707+58 is possibly another example of CEMP stars belonging to close binary systems. Lucatello et al. (2003) proposed that HE 0024–2523 underwent a past common-envelope phase with its companion that has become an AGB star. A similar past history may be applicable to SDSS 1707+58.

The stellar parameters of SDSS 1707+58 ($T_{\text{eff}} = 6700$ K and $\log g = 4.2$) are almost the same as those of HE 0024–2523 ($T_{\text{eff}} = 6625$ K and $\log g = 4.3$). On the other hand, the abundance ratios of the neutron-capture elements are different between these two stars – while HE 0024–2523 exhibits a very large excess of Pb ($[\text{Pb}/\text{Fe}] = +3.3$) and moderate over-abundances of Ba ($[\text{Ba}/\text{Fe}] = +1.46$), SDSS 1707+58 has a very large overabundance of Ba ($[\text{Ba}/\text{Fe}] = +3.40$). Our derived upper limit on the Pb abundance ratio of SDSS 1707+58 is still quite high ($[\text{Pb}/\text{Fe}] < +3.7$), so it does not constrain this comparison at present. We note that the possible close binary CS 22958–042 exhibits no excess of neutron-capture elements, but shows a large over-abundance of Na, as found also for SDSS 1707+58. Thus, large variations of chemical abundances are found even in these three (candidate) close binary systems. Further abundance measurements, as well as radial velocity monitoring, for SDSS 1707+58 are clearly desired to understand the evolution of such binary systems.

5. Kinematics

Table 11 provides kinematic data for our SDSS targets. Distances (expected to be accurate to on the order of 10-15%) for these stars are estimated using the methods described by Beers et al. (2000), under the assumption that they are main-sequence stars, as suggested by the surface gravities determined in this study. Proper motions are obtained based on the re-calibrated USNO-B2 catalog, as described by Munn et al. (2004), and are expected to be accurate to on the order of 3 mas/year. The radial velocities are taken from our high-resolution estimates listed in Table 1, with the exception of SDSS 1707+58, where we adopt the value measured from the SDSS spectrum. The space motions, errors in the space motions, and the other derived quantities listed in Table 11 are obtained following the procedures of Beers et al. (2000).

All six of the SDSS CEMP stars exhibit a derived r_{\max} (maximum distance from the Galactic center achieved during the course of their orbits) in excess of 10 kpc from the Galactic center. Four of the stars exhibit Z_{\max} (maximum height above or below the Galactic plane achieved during the course of their orbits) values larger than 10 kpc, or significant retrograde motions, indicating that these stars may belong to the outer-halo population of our Galaxy, according to the criteria of Carollo et al. (2007). This is also reminiscent of the apparent excess of CEMP stars with increasing distance from the plane reported by Frebel et al. (2006). Although the sample size is too small to derive any firm conclusions, the fraction of outer-halo stars among the CEMP stars appears to be quite high compared with the fraction found for metal-poor stars ($[\text{Fe}/\text{H}] < -2.2$) studied by Carollo et al. (2007). A comparison of the fraction of CEMP stars associated with the inner- and outer-halo populations, at a given metallicity, potentially constrains the initial mass function of early-generation stars, as discussed recently by Tumlinson (2007) and Komiya et al. (2007), and is clearly of interest for additional study, in particular given the very large samples of CEMP stars identified in SDSS/SEGUE.

6. Concluding remarks

Chemical compositions of seven CEMP turn-off stars are determined. Six stars among them exhibit a large excess of Ba, signature of a contribution by the nucleosynthesis in an AGB star. The distribution of carbon abundances in these stars suggest that the surface of such stars preserves the material transferred from the AGB star that was the erstwhile primary star in a binary system. If this is the case, the relatively wide distribution of Ba abundances ($[\text{Ba}/\text{H}]$) indicates a diversity of the efficiency of the s-process in metal-poor AGB stars. Further studies to identify the physical mechanism that produces such diversity are clearly desired.

The present study is the first application of high-resolution spectroscopy to candidate CEMP stars from the SDSS and SEGUE sample. Comparisons of our results on stellar parameters and chemical abundances with the estimates from the SDSS spectra confirmed that the selection of metal-poor stars works well in general. The SDSS/SEGUE survey is providing a large sample of candidate metal-poor stars. High-resolution spectroscopy for such stars in the near future will reveal the chemical abundance trends in the lowest metallicity range, as well as be useful for exploring the possible dependence of their chemical properties on their derived kinematics.

Funding for the SDSS and SDSS-II has been provided by the Alfred P. Sloan Foundation, the Participating Institutions, the National Science Foundation, the U.S. Department of Energy, the National Aeronautics and Space Administration, the Japanese Monbukagakusho, the Max Planck Society, and the Higher Education Funding Council for England. The SDSS Web Site is <http://www.sdss.org/>.

The SDSS is managed by the Astrophysical Research Consortium for the Participating Institu-

tions. The Participating Institutions are the American Museum of Natural History, Astrophysical Institute Potsdam, University of Basel, University of Cambridge, Case Western Reserve University, University of Chicago, Drexel University, Fermilab, the Institute for Advanced Study, the Japan Participation Group, Johns Hopkins University, the Joint Institute for Nuclear Astrophysics, the Kavli Institute for Particle Astrophysics and Cosmology, the Korean Scientist Group, the Chinese Academy of Sciences (LAMOST), Los Alamos National Laboratory, the Max-Planck-Institute for Astronomy (MPIA), the Max-Planck-Institute for Astrophysics (MPA), New Mexico State University, Ohio State University, University of Pittsburgh, University of Portsmouth, Princeton University, the United States Naval Observatory, and the University of Washington.

W. A. is supported by a Grant-in-Aid for Science Research from JSPS (grant 18104003). T. C. B., B. M., and T. S. acknowledge support by the US National Science Foundation under grants AST 04-06784 and AST 07-07776, as well as from grant PHY 02-16783; Physics Frontier Center/Joint Institute for Nuclear Astrophysics (JINA). D. C. is grateful to JINA for support of her long-term visitor status at Michigan State University, where the kinematical analysis took place. J.E.N. acknowledges support from the Australian Research Council under grant DP0663562.

REFERENCES

- Adelman-McCarthy, J. K., et al. 2007, *ApJS*, 172, 634
- Alonso, A., Arribas, S., & Martínez-Roger, C. 1996, *A&A*, 313, 873
- Alvarez, R., & Plez, B. 1998, *A&A*, 330, 1109
- Aoki, W., et al. 2005, *ApJ*, 632, 611
- Aoki, W., Beers, T. C., Christlieb, N., Norris, J. E., Ryan, S. G., & Tsangarides, S. 2007, *ApJ*, 655, 492
- Aoki, W., Norris, J. E., Ryan, S. G., Beers, T. C., & Ando, H. 2002a, *ApJ*, 567, 1166
- Aoki, W., Norris, J. E., Ryan, S. G., Beers, T. C., & Ando, H. 2002b, *PASJ*, 54, 933
- Aoki, W., Ryan, S. G., Norris, J. E., Beers, T. C., Ando, H., & Tsangarides, S. 2002c, *ApJ*, 580, 1149
- Asplund, M. 2005a, *ARA&A*, 43, 481
- Asplund, M., Grevesse, N., & Sauval, A. J. 2005b, *ASP Conf. Ser.* 336: *Cosmic Abundances as Records of Stellar Evolution and Nucleosynthesis*, 336, 25
- Barklem, P. S., & Aspelund-Johansson, J. 2005, *A&A*, 435, 373
- Barklem, P. S., & O’Mara, B. J. 1998, *MNRAS*, 300, 863

- Beers, T. C., & Christlieb, N. 2005, *ARA&A*, 43, 531
- Beers, T. C., Preston, G. W., & Shectman, S. A. 1992, *AJ*, 103, 1987
- Beers, T. C., et al. 2000, *AJ*, 119, 2866
- Beers, T.C., et al. 2006, *BAAS* 38, 168.08
- Beers, T. C., et al. 2007, *ApJS*, 168, 128
- Bond, H. E. 1974, *ApJ*, 194, 95
- Busso, M., Gallino, R., Lambert, D. L., Travaglio, C., & Smith, V. V. 2001, *ApJ*, 557, 802
- Busso, M., Gallino, R., & Wasserburg, G. J. 1999, *ARA&A*, 37, 239
- Carollo, D., et al. 2007, *Nature*, 450, 1020
- Castelli, F., & Kurucz, R. L. 2003, *Modelling of Stellar Atmospheres*, 210, 20P
- Charbonnel, C., & Zahn, J.-P. 2007, *A&A*, 467, L15
- Christlieb, N., et al. 2002, *Nature*, 419, 904
- Cohen, J. G., Christlieb, N., Qian, Y.-Z., & Wasserburg, G. J. 2003, *ApJ*, 588, 1082
- Cohen, J. G., et al. 2004, *ApJ*, 612, 1107
- Cohen, J. G., et al. 2006, *AJ*, 132, 137
- Collet, R., Asplund, M., & Thévenin, F. 2005, *A&A*, 442, 643
- Collet, R., Asplund, M., & Trampedach, R. 2006, *ApJ*, 644, L121
- Cui, W., & Zhang, B. 2006, *MNRAS*, 368, 305
- Denissenkov, P. A., & Pinsonneault, M. 2007, *ArXiv e-prints*, 709, arXiv:0709.4240
- Downes, R.A., et al. 2004, *AJ*, 127, 2838
- Frebel, A., et al. 2005, *Nature*, 434, 871
- Frebel, A., et al. 2006, *ApJ*, 652, 1585
- Fukugita, M., Ichikawa, T., Gunn, J.E., Doi, M., Shimasaku, K., & Schneider, D.P. 1996, *AJ*, 111, 1748
- Gunn, J.E., et al. 1998, *AJ*, 116, 3040
- Gunn, J.E., et al. 2006, *AJ*, 131, 2332

- Hogg, D.W., Finkbeiner, D.P., Schlegel, D.J., & Gunn, J.E. 2001, *AJ*, 122, 2129
- Ivans, I. I., Sneden, C., Gallino, R., Cowan, J. J., & Preston, G. W. 2005, *ApJ*, 627, L145
- Ivezic, Z., et al. 2004, *AN*, 325, 583
- Jonsell, K., Barklem, P. S., Gustafsson, B., Christlieb, N., Hill, V., Beers, T. C., & Holmberg, J. 2006, *A&A* 451, 651
- Keenan, P. C., *ApJ*, 96, 101
- Kim, Y.-C., Demarque, P., Yi, S. K., & Alexander, D. R. 2002, *ApJS*, 143, 499
- Komiya, Y., Suda, T., Minaguchi, H., Shigeyama, T., Aoki, W., & Fujimoto, M. Y. 2007, *ApJ*, 658, 367
- Kupka, F., Piskunov, N., Ryabchikova, T. A., Stempels, H. C., & Weiss, W. W. 1999, *A&AS*, 138, 119
- Kurucz, R. L. 1993, CD-ROM 13, ATLAS9 Stellar Atmospheres Programs and 2 km/s Grid (Cambridge: Smithsonian Astrophys. Obs.)
- Lawler, J. E., Bonvallet, G., & Sneden, C. 2001, *ApJ*, 556, 452
- Lee, Y.S., et al. 2007a, *AJ*, submitted
- Lee, Y.S., et al. 2007b, *AJ*, submitted
- Lucatello, S., Beers, T. C., Christlieb, N., Barklem, P. S., Rossi, S., Marsteller, B., Sivarani, T., & Lee, Y. S. 2006, *ApJ*, 652, L37
- Lucatello, S., Gratton, R., Cohen, J. G., Beers, T. C., Christlieb, N., Carretta, E., & Ramírez, S. 2003, *AJ*, 125, 875
- Lucatello, S., Tsangarides, S., Beers, T. C., Carretta, E., Gratton, R. G., & Ryan, S. G. 2005, *ApJ*, 625, 825
- Lupton, R., Gunn, J. E., Ivezić, Z., Knapp, G. R., & Kent, S. 2001, *Astronomical Data Analysis Software and Systems X*, 238, 269
- Margon, B., et al. 2002, *AJ*, 124, 1651
- Marsteller, B. 2007, PhD Thesis, Michigan State University
- Marsteller, B., et al. 2006, *BAAS*, 38, 242.02
- Masseron, T., et al. 2006, *A&A*, 455, 1059
- McWilliam, A. 1998, *AJ*, 115, 1640

- Munn, J. A., et al. 2004, *AJ*, 127, 3034
- Munari, U., & Zwitter, T. 1997, *A&A*, 318, 269
- Noguchi, K. et al. 2002, *PASJ*, 54, 855
- Norris, J. E., Ryan, S. G., & Beers, T. C. 1997a, *ApJ*, 488, 350
- Norris, J. E., Ryan, S. G., & Beers, T. C. 1997b, *ApJ*, 489, L169
- Norris, J. E., Ryan, S. G., & Beers, T. C. 2001, *ApJ*, 561, 1034
- Norris, J. E., Christlieb, N., Korn, A. J., Eriksson, K., Bessell, M. S., Beers, T. C., Wisotzki, L., & Reimers, D. 2007, *ApJ*, 670, 774
- Preston, G. W., & Sneden, C. 2001, *AJ*, 122, 1545
- Pier, J.R., Munn, J.A., Hindsley, R.B., Hennessy, G.S., Kent, S.M., Lupton, R.H., & Ivezić, Z. 2003, *AJ*, 125, 1559
- Plez, B., & Cohen, J. G. 2005, *A&A*, 434, 1117
- Reyniers, M., Van Winckel, H., Gallino, R., & Straniero, O. 2004, *A&A*, 417, 269
- Schlegel, D., Finkbeiner, D., & Davis, M. 1998, *ApJ*, 500, 525
- Smith, J.A., et al. 2002, *AJ*, 123, 2121
- Sneden, C., et al. 2003, *ApJ*, 591, 936
- Simons, J.W., Palmer, B.A., Hof, D.E., & Oldenborg, R.C. 1989, *J. Opt. Soc. Am. B.*, 6, 1097
- Sivarani, T., et al. 2006, *A&A*, 459, 125
- Skrutskie, M. F., et al. 2006, *AJ*, 131, 1163
- Stancliffe, R. J., Glebbeek, E., Izzard, R. G., & Pols, O. R. 2007, *A&A*, 464, L57
- Stoughton, C., et al. 2002, *AJ*, 123, 485
- Thompson, I. B., et al. 2007, *ApJ*, in press, ArXiv e-prints, 712, arXiv:0712.3228
- Tucker, D., et al. 2006, *AN*, 327, 821
- Tumlinson, J. 2007, *ApJ*, 664, L63
- van den Hoek, L. B., & Groenewegen, M. A. T. 1997, *A&AS*, 123, 305
- York, D.G., et al. 2000, *AJ*, 120, 1579

Zhao, C., & Newberg, H.J. 2006, unpublished manuscript (astro-ph/0612034)

Table 1. PROGRAM STARS AND OBSERVATIONS

Star	IAU Name	Exp. ^a	Counts ^b	Obs. date (JD)	V_{helio} (km s ⁻¹)
LP 706-7		20	16500	14 Sep 2006 (2453992.87)	80.35 ± 0.10
CS 29526-110		40	8000	10 Feb 2007 (2454141.72)	203.09 ± 0.39
SDSS 0036-10	SDSS J003602.17-104336.3	120	5350	14 Sep 2006 (2453992.95)	-146.18 ± 0.18
SDSS 0126+06	SDSS J012617.95+060724.8	120	5150	14 Sep 2006 (2453993.04)	-272.24 ± 0.28
SDSS 0817+26	SDSS J081754.93+264103.8	94	1050	10 Feb 2007 (2454141.76)	1.74 ± 2.52
SDSS 0924+40	SDSS J092401.85+405928.7	160	5250	10 Feb 2007 (2454141.87)	-366.16 ± 0.23
SDSS 1707+58	SDSS J170733.93+585059.7	117	2300	10 Feb 2007 (2454142.10)	...
SDSS 2047+00	SDSS J204728.84+001553.8	160	3000	14 Sep 2006 (2453992.75)	-417.92 ± 0.20

^aExposure time (minutes)

^bThe photon counts per pixel (0.18 km s⁻¹) at 5100 Å

Table 2. PHOTOMETRY DATA

object	V^a	$\sigma(V)$	$B - V^a$	$\sigma(B - V)$	K	$\sigma(K)$	$E(B - V)^b$	$E(B - V)^b$	$T_{\text{eff}}(V - K)$	$T_{\text{eff}}(B - V)$
LP 706-7	12.098	0.001	0.467	0.003	10.771	0.017	0.022	0.007	6206	5933
CS 29526-110	13.352	0.004	0.356	0.007	12.367	0.023	0.033	0.025	6800	6500
SDSS 0036-10	15.540	0.004	0.320	0.006	14.388	0.080	0.027	0.010	6500	6600
SDSS 0126+06	15.525	0.004	14.468	0.077	0.029	0.094	6600	...
SDSS 0817+26	15.990	0.004	0.43	0.006	14.707	0.077	0.024	0.028	6302	6097
SDSS 0924+40	15.480	0.004	0.42	0.006	14.165	0.053	0.014	...	6184	6097
SDSS 1707+58	15.810	0.004	0.33	0.006	14.776	0.108	0.035	0.091	6700	6600
SDSS 2047+00	16.009	0.004	0.390	0.006	14.880	0.120	0.088	0.126	6800	6600

^a V and $B - V$ for SDSS/SEGUE objects are already extinction and reddening corrected

^b $E(B - V)$ from the dust map of Schlegel et al. (1998)

^c $E(B - V)$ from the Na I D1 line

Table 3. RADIAL VELOCITY VARIATION FOUND FOR SDSS 1707+58

UT	HJD	exposure (minutes)	Shift (km s ⁻¹)	Width (mÅ)	V _{helio} (km s ⁻¹)
10 Feb.2007, 14:19	2454142.097	40	35.4	27.5	40.7
10 Feb.2007, 15:00	2454142.125	40	16.9	35.5	22.2
10 Feb.2007, 15:41	2454142.153	37	-2.3	23.3	3.0
11 Feb.2007, 15:34	2454143.148	20	15.6	16.9	20.8
11 Feb.2007, 15:49	2454143.159	20	16.5	20.0	21.7

Table 4. EQUIVALENT WIDTHS

Species	Wavelength (Å)	L.E.P. (eV)	log gf	Equivalent width (mÅ)							
				LP 706-7	CS 29526-110	SDSS 0036-10	SDSS 0126+06	SDSS 0817+26	SDSS 0924+40	SDSS 1707+58	SDSS 2047+00
Na I	5889.95	0.00	0.10	164.2	98.6	116.1	75.3	...	147.3	313.8	69.5
Na I	5895.92	0.00	-0.20	135.5	77.0	96.4	55.5	...	127.3	277.6	...
Mg I	4057.50	4.35	-0.89	13.0
Mg I	4571.10	0.00	-5.69	1.9
Mg I	5172.69	2.71	-0.38	129.6	117.6	99.8	84.9	71.8	120.2	184.2	124.9
Mg I	5183.60	2.72	-0.16	147.5	135.2	122.0	101.6	77.3	141.4	196.5	147.3
Mg I	5528.40	4.35	-0.49	33.0	28.8	22.7	11.2	22.0	28.7	...	40.7
Ca I	4226.73	0.00	0.24	122.1	...
Ca I	4435.69	1.89	-0.52	13.8	17.9	7.1	27.7
Ca I	4454.78	1.90	0.26	35.8	41.0	38.0	41.2	...	49.3
Ca I	4455.89	1.90	-0.53	10.3	12.4	8.7	12.9	...	13.0
Ca I	5265.56	2.52	-0.11	6.3	...	6.8	7.3
Ca I	5588.76	2.53	0.36	12.5	...	13.0	12.8
Ca I	5594.47	2.52	0.10	13.5	17.4	10.6	13.0
Ca I	5598.49	2.52	-0.09	6.3	...	7.5	19.7
Ca I	5857.45	2.93	0.24	5.9	18.3
Ca I	6102.72	1.88	-0.77	4.3	15.7
Ca I	6122.22	1.89	-0.32	12.7	16.5	21.1
Ca I	6162.17	1.90	-0.09	19.2	22.3	21.5
Ca I	6439.07	2.53	0.39	16.8	19.1	17.7	...	26.2
Ca I	6462.57	2.52	0.26	13.0	13.1	13.1	16.5
Ti I	4981.73	0.85	0.56	9.9	9.1
Ti I	4991.07	0.84	0.44	6.8
Ti I	4999.50	0.83	0.31	8.2	11.9
Ti I	5007.21	0.82	0.17	8.6	14.4
Ti I	5064.65	0.05	-0.94	4.6
Cr I	4652.16	1.00	-1.03	4.1
Cr I	5206.04	0.94	0.02	21.0	...	14.6	13.4	...	26.2
Cr I	5208.44	0.94	0.16	23.5	31.9	22.5	25.9	...	37.4
Fe I	4063.59	1.56	0.06	88.2 ^a
Fe I	4071.74	1.61	-0.02	82.1	90.4	75.8	...	56.5	74.8	...	74.5
Fe I	4107.49	2.83	-0.88	10.6	20.7
Fe I	4143.41	3.05	-0.20	17.9	19.3	19.2	27.0	...	23.8

Table 4—Continued

Species	Wavelength (Å)	L.E.P. (eV)	log gf	Equivalent width (mÅ)							
				LP 706-7	CS 29526-110	SDSS 0036-10	SDSS 0126+06	SDSS 0817+26	SDSS 0924+40	SDSS 1707+58	SDSS 2047+00
Fe I	4143.87	1.56	-0.51	61.5	68.6	59.2	26.9	...	62.1	...	59.6
Fe I	4202.03	1.49	-0.71	43.3	...
Fe I	4271.76	1.49	-0.16	38.1	...
Fe I	4307.90	1.56	-0.07	62.1	...
Fe I	4325.76	1.61	0.01	65.0	...
Fe I	4383.54	1.49	0.20	98.9 ^a	102.5	87.1	69.4	...	102.2	91.0	99.6
Fe I	4404.75	1.56	-0.14	77.6	84.7	65.4	56.4	41.5	52.6	66.7	76.9
Fe I	4415.12	1.61	-0.62	67.5	65.4	59.5	22.7	21.0	85.3	37.2	65.9
Fe I	4427.31	0.05	-2.92	36.0	19.7	29.3	68.0	...	39.7
Fe I	4442.34	2.20	-1.25	...	19.4	22.3	19.5
Fe I	4447.72	2.22	-1.34	...	7.1
Fe I	4459.12	2.18	-1.28	14.2	15.6	11.8	14.9	...	22.1
Fe I	4461.65	0.09	-3.21	13.2	12.5	...	22.1
Fe I	4466.55	2.83	-0.60	14.5	22.9	17.4	17.8 ^a	...	12.6
Fe I	4476.02	2.85	-0.82	13.3	...	7.5	11.6
Fe I	4494.56	2.20	-1.14	15.3	9.0	11.9	15.2
Fe I	4528.61	2.18	-0.82	29.6	42.7	22.6	29.8	...	28.7
Fe I	4531.15	1.49	-2.15	10.7
Fe I	4592.65	1.56	-2.45	4.9
Fe I	4602.94	1.49	-2.21	6.8	11.5
Fe I	4871.32	2.87	-0.36	...	17.2
Fe I	4872.14	2.88	-0.57	13.3	12.9	9.6	16.1
Fe I	4890.75	2.88	-0.39	22.2	28.9	11.1	19.5	...	28.4
Fe I	4891.49	2.85	-0.11	31.8	34.5	21.9	36.5	...	31.5
Fe I	4903.31	2.88	-0.93	5.2	9.4	17.4
Fe I	4918.99	2.87	-0.34	19.7	24.4	21.1	...	28.8
Fe I	4920.50	2.83	0.07	40.3	54.7	31.8	40.2	...	46.5
Fe I	4957.30	2.85	-0.41	22.7	21.8
Fe I	4957.60	2.81	0.23	49.7	61.9	42.2	...	23.8	42.2
Fe I	4966.09	3.33	-0.87	5.1	6.2
Fe I	4994.13	0.92	-2.96	4.2
Fe I	5006.12	2.83	-0.61	13.5	12.9	14.2
Fe I	5012.07	0.86	-2.64	10.7	...	8.6	19.9
Fe I	5041.76	1.49	-2.20	...	28.8 ^a	11.4

Table 4—Continued

Species	Wavelength (Å)	L.E.P. (eV)	log gf	Equivalent width (mÅ)							
				LP 706-7	CS 29526-110	SDSS 0036-10	SDSS 0126+06	SDSS 0817+26	SDSS 0924+40	SDSS 1707+58	SDSS 2047+00
Fe I	5049.82	2.28	-1.34	10.0	9.9	14.8
Fe I	5051.63	0.92	-2.80	6.5	15.2 ^a	...	10.0
Fe I	5151.91	1.01	-3.32	7.7 ^a
Fe I	5171.60	1.49	-1.79	16.8	14.3	13.8	...	23.2
Fe I	5191.46	3.04	-0.55	10.7	26.5	9.0	13.1	...	17.2
Fe I	5192.34	3.00	-0.42	14.4 ^a	15.7	11.0	16.7	...	20.8
Fe I	5194.94	1.56	-2.09	9.5	...	14.6	8.9
Fe I	5198.71	2.22	-2.13	2.2
Fe I	5202.34	2.18	-1.84	4.4
Fe I	5216.27	1.61	-2.15	7.5
Fe I	5232.94	2.94	-0.06	28.7	32.6	19.5	29.6	...	39.2
Fe I	5266.56	3.00	-0.39	14.9	20.5	14.3	15.2	...	16.9
Fe I	5269.54	0.86	-1.32	67.4	64.6	57.4	17.7	42.4	58.0	39.4	74.5
Fe I	5270.36	1.61	-1.34	36.0	40.9	29.8	37.3	...	57.5 ^a
Fe I	5281.79	3.04	-0.83	4.7
Fe I	5324.18	3.21	-0.10	16.4	23.8	14.4	17.7	...	23.8
Fe I	5328.04	0.92	-1.47	57.4	57.9	45.9	-1.47	13.4	50.4	40.6	67.7
Fe I	5328.53	1.56	-1.85	14.4	13.1	11.5	10.2	...	19.7
Fe I	5339.93	3.27	-0.65	7.9
Fe I	5455.61	1.01	-2.10	27.5	30.7	22.1	34.9
Fe I	5497.52	1.01	-2.85	4.9
Fe I	5506.78	0.99	-2.80	6.5
Fe I	5569.62	3.42	-0.54	6.2	10.7	11.1
Fe I	5572.84	3.40	-0.28	8.7	13.9	13.0	...	15.8
Fe I	5586.75	3.37	-0.10	12.6	17.2	8.5	14.4	...	17.5
Fe I	5615.64	3.33	0.05	18.2	23.5	14.2	20.9	...	24.1
Fe I	6136.61	2.45	-1.40	6.9
Fe I	6137.69	2.59	-1.40	6.9
Fe I	6191.56	2.43	-1.42	6.4
Fe I	6230.72	2.56	-1.28	6.2	9.4
Fe I	6393.60	2.43	-1.43	5.8
Fe I	6677.99	2.69	-1.42	4.8
Co I	4121.32	0.92	-0.32	10.6	...	7.7
Ni I	5476.91	1.83	-0.89	11.9	21.0	5.7	11.9	...	16.5

Table 4—Continued

Species	Wavelength (Å)	L.E.P. (eV)	log gf	Equivalent width (mÅ)							
				LP 706-7	CS 29526-110	SDSS 0036-10	SDSS 0126+06	SDSS 0817+26	SDSS 0924+40	SDSS 1707+58	SDSS 2047+00
Zn I	4722.15	0.00	-0.37	3.0
Sc II	4320.75	0.61	-0.25	11.5	19.4
Ti II	4395.00	1.08	-0.51	42.3	...
Ti II	4443.77	1.08	-0.70	35.8	45.6	33.3	18.1	...	42.2	...	46.1
Ti II	4444.54	1.12	-2.21	5.1
Ti II	4450.50	1.08	-1.51	6.9	12.2	14.3
Ti II	4464.46	1.16	-2.08	5.4	6.6
Ti II	4468.52	1.13	-0.60	39.4	52.7	37.6	29.3	...	38.1	...	57.5
Ti II	4501.27	1.12	-0.76	29.8	44.4	29.2	20.1	...	29.8	...	47.0
Ti II	4533.97	1.24	-0.77	37.1	47.6	34.6	37.7	33.2	57.0
Ti II	4563.77	1.22	-0.96	24.5	29.7	29.8	13.9	...	24.3	31.2	27.6
Ti II	4571.96	1.57	-0.53	29.6	...	33.9	41.8	33.0	...
Ti II	4589.92	1.24	-1.79	11.1
Ti II	4805.09	2.06	-1.10	...	9.6	8.7
Ti II	5226.53	1.57	-1.30	6.5	...	9.5	8.3	...	16.0
Fe II	4491.40	2.86	-2.70	3.9	10.6
Fe II	4508.28	2.86	-2.58	7.4	13.4	12.8
Fe II	4515.34	2.84	-2.48	...	9.9
Fe II	4520.23	2.81	-2.60	4.5	9.1
Fe II	4522.63	2.84	-2.03	10.0	...	11.9	17.5	...	17.9
Fe II	4555.89	2.83	-2.29	...	20.3	17.1
Fe II	4583.83	2.81	-2.02	17.1	42.7	20.1	22.1	26.8
Fe II	4923.93	2.89	-1.32	34.2	63.4	32.6	15.7	23.9	46.8
Fe II	5018.45	2.89	-1.22	41.4	68.5	43.1	21.7	...	45.4	47.3	57.2
Fe II	5197.56	3.23	-2.10	3.5	14.1	8.1
Fe II	5234.62	3.22	-2.27	4.8	12.9
Fe II	5276.00	3.20	-1.94	7.4	18.0	10.9	17.7
Fe II	5316.62	3.15	-1.85	9.5	29.3	10.6	...	17.0
Sr II	4077.71	0.00	0.15	74.1	129.9	60.4	102.7	...	91.5	287.1	104.5
Sr II	4215.52	0.00	-0.18	63.5	111.0	43.9	92.6	43.7	82.8	160.9	99.0
Y II	4204.69	0.00	-1.76	61.5	...	55.5	25.2	...	101.2
Y II	4883.68	1.08	0.07	...	15.1	12.7
Y II	4900.12	1.03	-0.09	...	47.1	35.6	...
Zr II	4048.67	0.80	-0.48	...	14.8

Table 4—Continued

Species	Wavelength (Å)	L.E.P. (eV)	log gf	Equivalent width (mÅ)							
				LP 706–7	CS 29526–110	SDSS 0036–10	SDSS 0126+06	SDSS 0817+26	SDSS 0924+40	SDSS 1707+58	SDSS 2047+00
Zr II	4149.20	0.80	-0.03	...	31.9	...	20.0	...	32.6	...	24.2
Zr II	4150.97	0.80	-1.08	4.2
Ba II	4554.03	0.00	0.16	152.3	140.8	51.2	88.9	282.2	108.1
Ba II	4934.09	0.00	-0.16	147.0 ^a	169.5	34.1	127.9	...	126.9	248.2	102.8
Ba II	5853.70	0.60	-1.01	48.1	77.8	9.0	38.6	...	37.8	77.6	30.2
Ba II	6141.70	0.70	-0.07	92.4	123.4	12.7	85.3	...	78.4	192.0	74.4
Ba II	6496.91	0.60	-0.38	81.8	115.8	8.6	88.6	...	68.3	150.3	63.5
La II	4086.71	0.00	-0.07	23.1	41.5	...	16.5	8.0
La II	4123.22	0.32	0.13	21.4	43.2	...	16.7	12.7
Na I ^b	5889.95	0.00	0.10	27.6	90.6	38.9	259.0	252.0	100.0	...	319.0

^aEquivalent width measured, but not used in the analysis.

^bEquivalent width of interstellar absorption.

Table 5. RADIAL VELOCITIES FROM SDSS SPECTRA

Star	JD	V_{helio} (km s ⁻¹)	Remarks
SDSS 0036–10	2,452,146	-150.2 ± 2.4	SDSS
	2,452,162	-143.9 ± 1.9	SDSS
	2,453,993	-146.18 ± 0.18	this work
SDSS 0126+06	2,453,712	-267.1 ± 2.5	SDSS
	2,453,713	-273.8 ± 2.9	SDSS
	2,453,993	-272.24 ± 0.28	this work
SDSS 0817+26	2,452,709	45.8 ± 3.5	SDSS
	2,454,142	1.7 ± 2.5	this work
SDSS 0924+40	2,452,708	-365.5 ± 1.8	SDSS
	2,452,636	-369.5 ± 2.2	SDSS
	2,454,142	-366.16 ± 0.23	this work
SDSS 1707+58	2,451,703	37.2 ± 3.2	SDSS
SDSS 2047+00	2,452,466	-419.2 ± 2.3	SDSS
	2,452,524	-420.4 ± 1.9	SDSS
	2,452,932	-404.3 ± 2.3	SDSS
	2,453,993	-417.92 ± 0.20	this work

Table 6. ATMOSPHERIC PARAMETERS

Star	T_{eff} (K)	$\sigma(T_{\text{eff}})$ (K)	$\log g$ (dex)	$\sigma(\log g)$ (dex)	[Fe/H] (dex)	$\sigma([\text{Fe}/\text{H}])$ (dex)	v_{micro} km s ⁻¹	$\sigma(v_{\text{micro}})$ km s ⁻¹
LP 706–7	6200	150	4.3	0.3	-2.5	0.3	1.4	0.3
CS 29526–110	6800	150	4.1	0.3	-2.1	0.3	2.1	0.3
SDSS 0036–10	6500	200	4.5	0.3	-2.5	0.3	1.5	0.3
SDSS 0126+06	6600	200	4.1	0.3	-3.2	0.3	2.0	0.5
SDSS 0817+26	6300	150	4.0	0.5	-3.2	0.3	1.5	0.5
SDSS 0924+40	6200	150	4.0	0.3	-2.6	0.3	1.4	0.3
SDSS 1707+58	6700	200	4.2	0.3	-2.5	0.3	1.5	0.5
SDSS 2047+00	6600	200	4.5	0.3	-2.1	0.3	1.3	0.3

Table 7. CHEMICAL ABUNDANCES RESULTS

	FeI	FeII	Li	C	Na I	MgI	CaI	ScII	TiI	TiII	CrI	CoI	NiI	ZnI	SrII	YII	ZrII	BaII	LaII	Pb I
Sun																				
log(A)	7.45	7.45	1.05	8.39	6.17	7.53	6.31	3.05	4.90	4.90	5.64	4.92	6.23	4.60	2.92	2.21	2.59	2.17	1.13	2.00
LP 706-7																				
log $\epsilon(X)$	4.92	4.92	2.3	8.00	4.76	5.42	4.00	0.72	2.92	2.76	3.04	2.60	3.77	2.07	0.47	1.72	0.52	2.0
[X/Fe]	-2.53	-2.53	...	2.14	1.12	0.42	0.22	0.20	0.55	0.39	-0.07	0.21	0.07	0.00	0.08	2.08	1.92	2.53
N	59	11	1		2	5	13	1	5	9	3	1	1	1	2	4	2	1
σ	0.12	0.12	0.2	0.25	0.25	0.13	0.09	0.18	0.14	0.12	0.14	0.19	0.18	0.13	0.22	0.18	0.16	
CS 29526-110																				
log $\epsilon(X)$	5.39	5.38	< 2.3	8.4	4.25	5.69	4.45	...	3.39	3.08	3.53	...	4.52	...	1.63	1.50	1.80	2.5	1.16	3.1
[X/Fe]	-2.06	-2.07		2.07	0.14	0.22	0.19	...	0.54	0.24	-0.05	...	0.35	...	0.77	1.34	1.26	2.39	2.09	3.16
N	40	11			2	4	8		2	7	1	...	1	...	2	2	2	4	2	1
σ	0.11	0.12		0.26	0.19	0.16	0.10	...	0.11	0.14	0.11	...	0.11	...	0.27	0.20	0.20	0.22	0.20	
SDSS 0036-10																				
log $\epsilon(X)$	5.04	5.03	< 2.0	8.30	4.54	5.37	4.16	3.00	3.05	2.73	3.65	...	0.24	0.05	...	< 2.3
[X/Fe]	-2.41	-2.42		2.32	0.78	0.25	0.26	0.51	-0.18	0.22	-0.17	...	-0.27	0.29	...	
N	33	5			2	3	9	8	2	1	1	...	2	4	...	
σ	0.17	0.15		0.32	0.32	0.19	0.13	0.15	0.16	0.18	0.15	...	0.29	0.24	...	
SDSS 0126+06																				
log $\epsilon(X)$	4.34	4.34	< 2.2	8.2	3.75	5.03	2.45	1.15	...	1.41	1.81	0.48	2.3
[X/Fe]	-3.11	-3.11		2.92	0.69	0.61	0.66	1.35	...	1.93	2.75	2.46	3.41
N	6	2			2	4	4	2	...	1	5	2	1
σ	0.16	0.14		0.32	0.20	0.18	0.14	0.37	...	0.19	0.30	0.16	
SDSS 0817+26																				
log $\epsilon(X)$	4.29	...	< 2.3	< 7.6	...	4.8	-0.1	-0.22		
[X/Fe]	-3.16	...		< 2.2	...	0.43	0.14	0.77	...	
N	5	3	1	1
σ	0.20	0.23	0.40	0.35
SDSS 0924+40																				
log $\epsilon(X)$	4.94	4.91	< 2.0	8.6	4.97	5.55	4.08	0.89	...	2.79	2.84	...	3.78	...	1.02	1.48	...	2.5
[X/Fe]	-2.51	-2.55		2.72	1.31	0.52	0.28	0.35	...	0.40	-0.29	...	0.05	...	0.60	1.81	...	3.01
N	33	4			2	4	6	1	...	9	2	...	1	...	2	5	...	1
σ	0.16	0.13		0.32	0.29	0.15	0.12	0.14	...	0.14	0.16	...	0.15	...	0.25	0.22	...	
SDSS 1707+58																				
log $\epsilon(X)$	4.93	4.96	< 2.5	8.0:	6.36	6.14	4.58	2.98	2.65	3.05		< 3.2

Table 7—Continued

	FeI	FeII	Li	C	Na I	MgI	CaI	ScII	TiI	TiII	CrI	CoI	NiI	ZnI	SrII	YII	ZrII	BaII	LaII	Pb I
[X/Fe]	-2.52	-2.49		+2.1:	2.71	1.13	0.79	0.60	2.25	3.40
N	9	3			2	2	1	4	2	5
σ	0.16	0.15		0.32	0.22	0.21	0.21	0.15	0.38	0.31
SDSS 2047+00																				
$\log \epsilon(X)$	5.40	5.40	< 2.3		4.45	5.75	4.59	...	3.66	3.29	3.49	...	4.26	...	1.56	0.95	1.5	1.62
[X/Fe]	-2.05	-2.05		2.00	0.33	0.27	0.32	...	0.80	0.44	-0.10	...	0.08	...	0.68	0.79	0.96	1.50
N	32	9			1	4	9	...	1	8	2	...	1	...	2	1	1	5
σ	0.15	0.13		0.32	0.28	0.18	0.13	...	0.15	0.15	0.15	...	0.15	...	0.29	0.24

Table 8. ABUNDANCE CHANGES BY CHANGING ATMOSPHERIC PARAMETERS

	LP 706–7					CS 29526–110			
	σT_{eff} 100 K	$\sigma \log g$ 0.3 dex	$\sigma [\text{Fe}/\text{H}]$ 0.3 dex	σv_{micro} 0.3 km s ⁻¹	Δ_{ATLAS}	σT_{eff} 100 K	$\sigma \log g$ 0.3 dex	$\sigma [\text{Fe}/\text{H}]$ 0.3 dex	σv_{micro} 0.3 km s ⁻¹
Fe I	0.08	-0.01	0.01	-0.02	-0.08	0.07	-0.01	0.01	-0.03
Fe II	0.01	0.10	0.00	-0.01	-0.06	0.02	0.10	0.00	-0.02
C (CH)	0.15	-0.10	0.00	0.00	-0.10	0.15	-0.12	0.01	0.00
Na I	0.11	-0.15	0.00	-0.05	-0.11	0.07	-0.03	0.00	-0.07
Mg I	0.04	-0.08	-0.02	-0.05	-0.13	0.06	-0.04	0.00	-0.06
Ca I	0.05	0.00	0.00	-0.01	-0.08	0.05	-0.01	0.00	-0.01
Ti I	0.08	0.00	0.01	0.00	-0.08	0.07	-0.01	0.01	0.00
Ti II	0.04	0.10	0.00	-0.02	-0.06	0.04	0.09	0.00	-0.02
Cr I	0.08	0.00	0.01	-0.01	-0.08	0.08	-0.01	0.01	-0.02
Ni I	0.08	0.01	0.01	-0.01	-0.07	0.07	-0.01	0.01	-0.01
Sr II	0.08	0.03	0.00	-0.16	-0.10	0.07	0.02	-0.01	-0.2
Ba II	0.09	-0.02	0.00	-0.10	-0.14	0.07	0.02	-0.02	-0.15
La II	0.06	0.10	0.00	-0.02	-0.06
Eu II	0.06	0.11	0.00	0.02	-0.05
Pb I	0.08	0.01	0.00	-0.01	-0.10	0.07	-0.01	0.01	-0.02

Table 9. COMPARISONS OF ATMOSPHERIC PARAMETERS AND ABUNDANCES WITH SDSS ESTIMATES

	T_{eff}		$\log g$		$[\text{Fe}/\text{H}]$		$[\text{C}/\text{Fe}]$	
	SDSS	this work	SDSS	this work	SDSS	this work	SDSS	this work
SDSS 0036–10	6595	6500	3.58	4.5	-2.49	-2.41	2.50	2.3
SDSS 0126+06	6970	6600	4.01	4.1	-2.68	-3.11	2.71	2.9
SDSS 0817+26	6213	6300	3.28	4.0:	-2.88	-3.16	1.19	< 2.2
SDSS 0924+40	6264	6200	3.67	4.0	-2.65	-2.51	2.58	2.7
SDSS 1707+58	6656	6700	3.19	4.2	-2.44	-2.52	2.27	2.1:
SDSS 2047+00	6489	6600	3.76	4.5	-2.22	-2.05	1.93	2.0

Table 10. ABUNDANCES RESULTS

	[Fe/H]	[C/Fe]	[N/Fe]	[Na/Fe]	[Mg/Fe]	[Ca/Fe]	[Sc/Fe]	[Ti/Fe]	[Cr/Fe]	[Ni/Fe]	[Zn/Fe]	[Sr/Fe]	[Ba/Fe]	[Pb/Fe]	Teff	logg	ref. ^a
LP 706-7	-2.53	2.14	1.20	0.60	0.42	0.22	0.20	0.47	-0.07	0.07	0.00	0.08	2.08	2.53	6300	4.30	1
CS 29526-110	-2.06	2.07	1.40	0.14	0.22	0.19	...	0.39	-0.05	0.35	...	0.77	2.39	3.16	6800	4.10	1
SDSS 0036-10	-2.41	2.32	...	0.78	0.25	0.26	...	0.51	-0.18	-0.17	...	-0.27	0.29	...	6500	4.50	1
SDSS 0126+06	-3.11	2.92	...	0.69	0.61	0.66	0.62	1.35	2.75	3.41	6600	4.10	1
SDSS 0924+40	-2.51	2.72	...	1.31	0.52	0.28	0.35	0.40	-0.29	0.05	...	0.60	1.81	3.10	6200	4.00	1
SDSS 1707+58	-2.52	2.1	...	2.71	1.13	0.79	...	0.60	2.25	3.40	...	6700	4.20	1
SDSS 2047+00	-2.05	2.	...	0.33	0.27	0.32	...	0.62	-0.10	0.08	...	0.68	1.50	...	6600	4.50	1
CS29528-028	-2.86	2.77	...	2.33	1.69	0.46	0.59	0.87	...	0.26	3.27	...	6800	4.00	2
CS22898-027	-2.26	2.20	0.90	0.33	0.41	0.40	...	0.41	-0.10	0.02	0.92	0.92	2.23	2.84	6250	3.70	3,4
CS29497-030	-2.57	2.47	2.12	0.58	0.44	0.47	0.67	0.64	0.03	0.04	...	0.84	2.32	3.55	7000	4.10	5
HE2148-1247	-2.32	1.91	1.65	...	0.50	0.45	0.59	0.55	-0.35	0.06	...	0.76	2.36	3.12	6380	3.90	6
HE0024-2523	-2.72	2.60	2.10	-0.17	0.73	0.66	0.37	0.85	-0.41	0.34	1.46	3.30	6625	4.30	7
HE22881-036	-2.06	1.96	1.00	0.16	0.40	0.62	...	0.33	0.59	1.93	...	6200	4.00	8
HE0007-1832	-2.65	2.55	1.85	...	0.76	0.32	...	0.39	...	0.02	0.16	...	6515	3.80	9
HE0338-3945	-2.42	2.13	1.55	0.36	0.30	0.38	0.53	0.37	-0.12	0.01	...	0.74	2.41	3.10	6160	4.13	10
HE1105+0027	-2.42	2.00	0.47	0.47	0.28	0.32	0.05	-0.29	2.45	...	6132	3.50	11
HE0143-0441	-2.31	1.98	1.73	...	0.63	0.43	0.67	0.40	-0.38	-0.31	0.46	0.86	2.32	3.11	6240	3.70	12
CS31080-095	-2.80	2.69	0.70	-0.48	0.65	0.17	-0.02	0.32	0.02	0.09	0.58	-0.41	0.77	...	6050	4.50	13
CS22958-042	-2.80	3.15	2.15	2.62	0.32	0.36	0.05	0.32	-0.15	-0.09	...	-0.20	6250	3.50	13
CS29528-041	-3.25	1.59	3.00	1.00	0.40	0.40	0.26	0.40	-0.17	0.00	...	-0.20	0.97	...	6150	4.00	13

^aReferences— (1)This work; (2)Aoki et al. (2007); (3)Aoki et al. (2002b); (4)Aoki et al. (2002c); (5)Ivans et al. (2005); (6)Cohen et al. (2003); (7)Lucatello et al. (2003); (8)Preston & Sneden (2001); (9)Cohen et al. (2004); (10)Jonsell et al. (2006); (11)Barklem & Aspelund-Johansson (2005); (12)Cohen et al. (2006); (13)Sivarani et al. (2006)

Table 11. KINEMATICS DATA

star	D (kpc)	V_{helio} (km s ⁻¹)	μ_{α} (mas/yr)	μ_{δ}	U	$\sigma(U)$	V	$\sigma(V)$	W	$\sigma(W)$	V_{ϕ}	$\sigma(V_{\phi})$	e	r_{min} (kpc)	r_{max} (kpc)	Z_{max} (kpc)	
								(km s ⁻¹)									
SDSS 0036-10	2.27	-146	-11	-50	-399	48	-403	47	2	17	-154	43	0.92	3	66	22	
SDSS 0126+06	1.75	-272	15	11	15	23	-99	19	298	13	120	19	0.41	9	22	20	
SDSS 0817+26	1.46	2	21	-10	-95	13	-78	20	111	19	139	20	0.38	5	12	5	
SDSS 0924+40	1.39	-366	-31	-46	-130	18	-293	35	-392	18	-73	35	0.74	8	54	53	
SDSS 1707+58	2.43	37	-2	1	5	33	30	20	46	27	242	20	0.24	8	13	2	
SDSS 2047+00	2.23	-418	20	-33	209	22	-510	32	-138	41	-326	32	0.66	6	31	9	

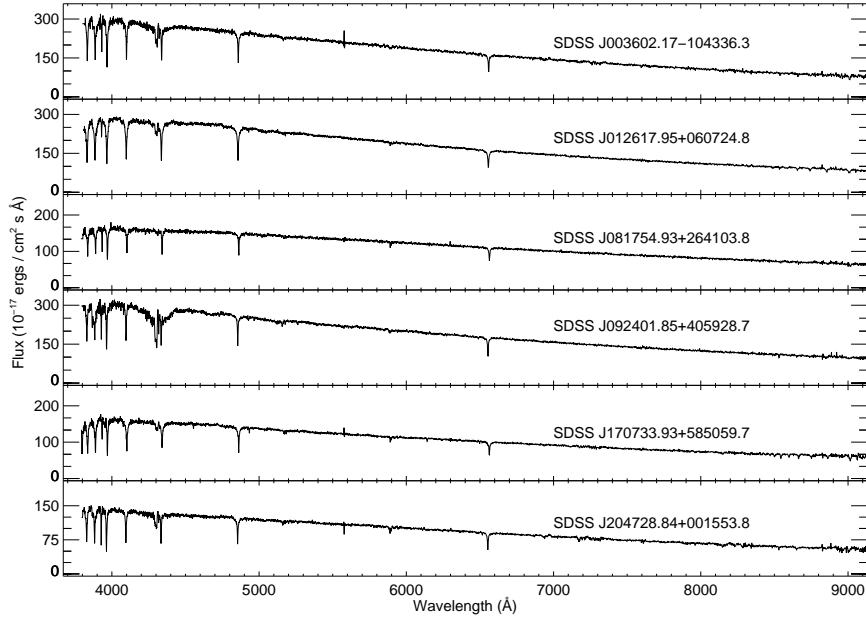


Fig. 1.— Medium-resolution, flux-calibrated SDSS spectra of our SDSS/SEGUE targets.

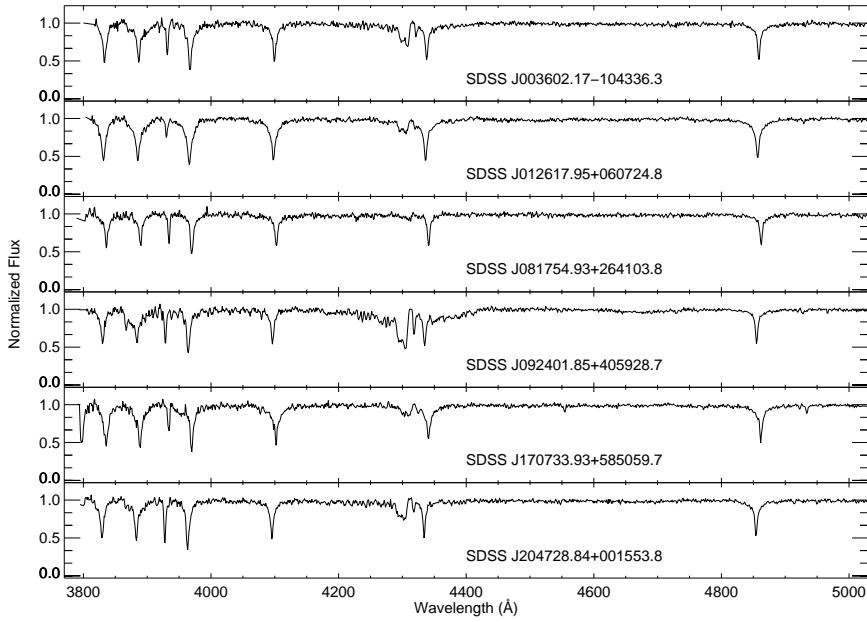


Fig. 2.— The blue range of the normalized SDSS spectra.

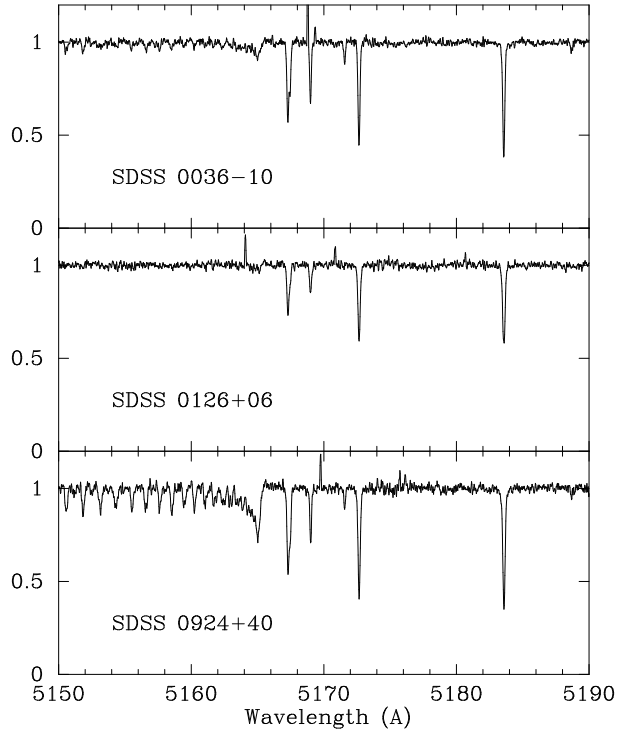


Fig. 3.— Examples of the Subaru spectra for the range including the C₂ Swan 0-0 band and the Mg I triplet.

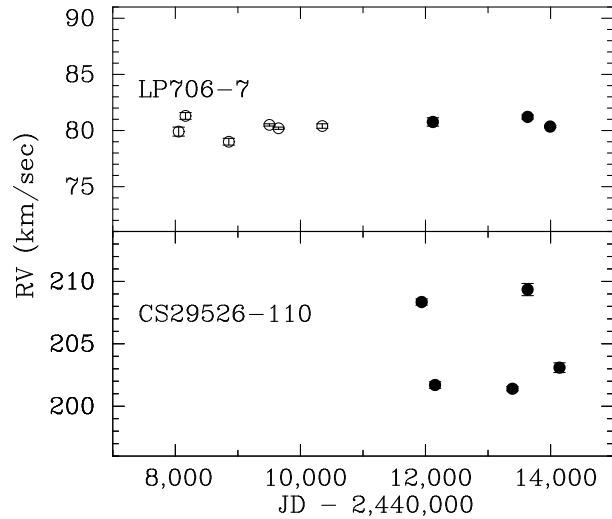


Fig. 4.— Radial velocity as a function of Julian Day number for LP 706-7 and CS 29526-110. The filled circles indicate our measurements with the Subaru Telescope, including the results by Aoki et al. (2002b), while open circles mean the results by Norris et al. (1997a) for LP 706-7 and by Aoki et al. (2002c) obtained with the William Herschel Telescope for CS 29526-110.

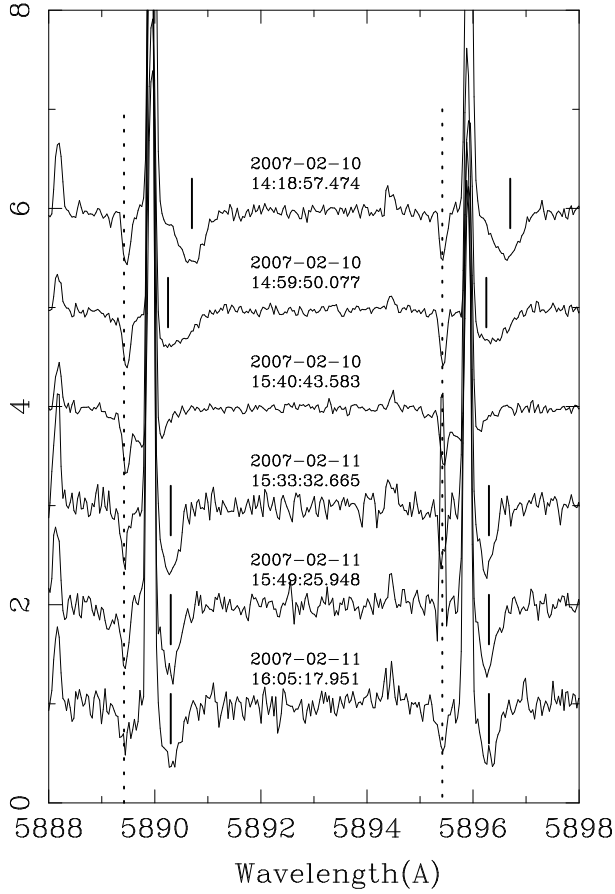


Fig. 5.— Spectra of the Na I D lines region for SDSS 1707+58 obtained by individual HDS exposures. The center of the exposure (UT) is presented for each spectrum. The exposure time is different between the two observing nights (see Table 3). The positions of interstellar Na I lines are shown by dotted lines, while the line positions of the stellar absorption are shown by solid lines. The emission from the Earth’s atmosphere and interstellar absorption show no variation in wavelengths, while the stellar absorption lines show rapid changes in the 10 February (UT) spectra.

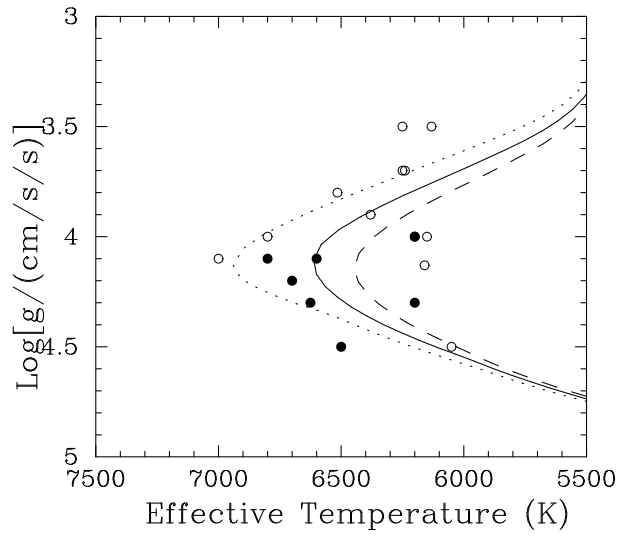


Fig. 6.— Surface gravity as a function of effective temperature for our sample (filled circles) and other CEMP turn-off stars from the literature given in Table 10 (open circles). The dotted, solid, and dashed lines indicate the isochrones of Kim et al. (2002) for $[\text{Fe}/\text{H}] = -2.5$, with ages of 10, 12, and 14 Gyr, respectively.

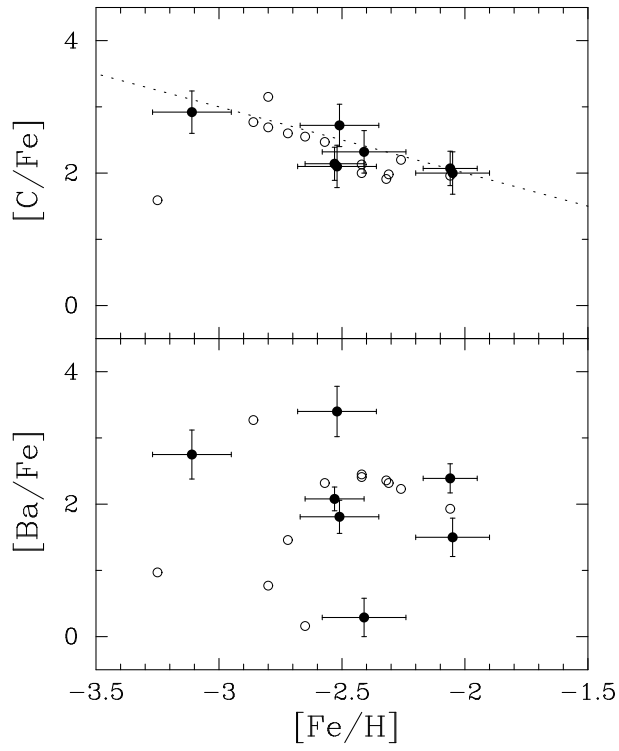


Fig. 7.— The abundance ratios of $[\text{C}/\text{Fe}]$ and $[\text{Ba}/\text{Fe}]$ as functions of $[\text{Fe}/\text{H}]$. Filled circles are objects studied by the present work, while open ones are from the literature given in Table 10. The dotted line in the upper panel means the line for $[\text{C}/\text{H}]=0$.

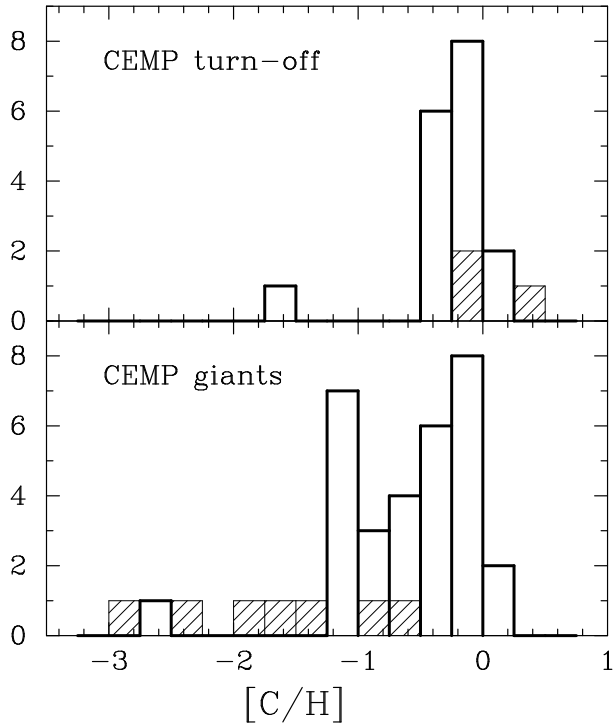


Fig. 8.— $[C/H]$ distributions for CEMP turn-off stars (upper) and giants (lower). See text for the selection criteria for these samples. The open histogram with strong lines indicates the objects having excesses of Ba ($[Ba/Fe] > +0.5$). The hatched one is for Ba-normal stars.

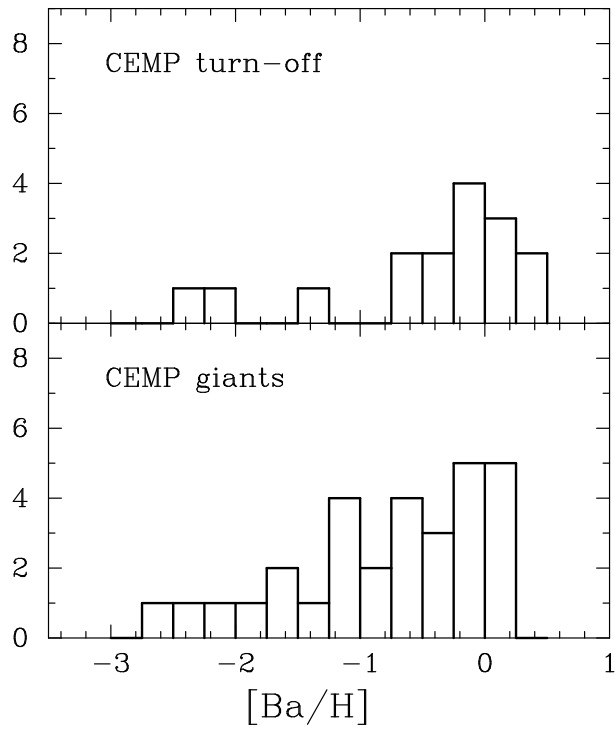


Fig. 9.— The same as Fig. 8, but for $[\text{Ba}/\text{H}]$. Only the histogram for Ba-enhanced ($[\text{Ba}/\text{Fe}] > +0.5$) stars are shown.

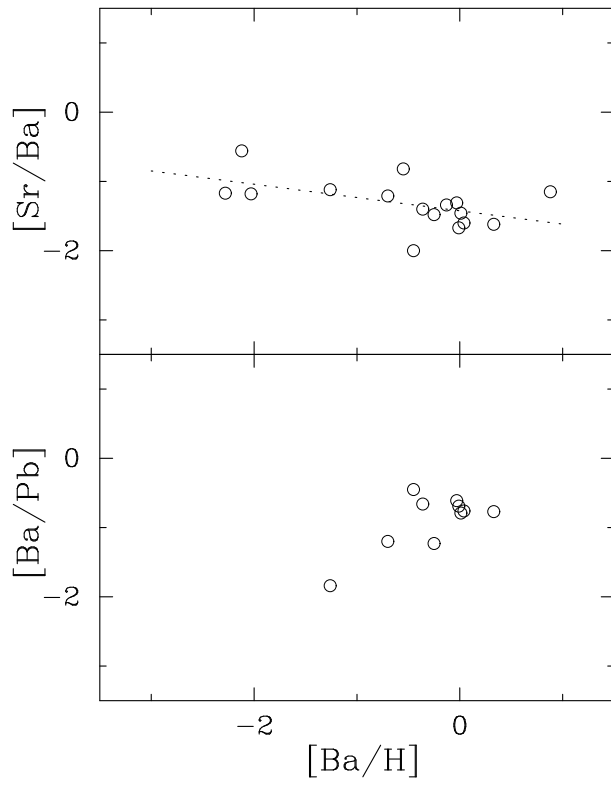


Fig. 10.— The abundance ratios of $[Sr/Ba]$ (upper) and $[Ba/Pb]$ (lower), as functions of $[Ba/H]$, for CEMP turn-off stars.